

2019

Developing green processes for the conversion of biobased materials into pyrones

William Bradley
Iowa State University

Follow this and additional works at: <https://lib.dr.iastate.edu/etd>

 Part of the [Organic Chemistry Commons](#)

Recommended Citation

Bradley, William, "Developing green processes for the conversion of biobased materials into pyrones" (2019). *Graduate Theses and Dissertations*. 17649.
<https://lib.dr.iastate.edu/etd/17649>

This Dissertation is brought to you for free and open access by the Iowa State University Capstones, Theses and Dissertations at Iowa State University Digital Repository. It has been accepted for inclusion in Graduate Theses and Dissertations by an authorized administrator of Iowa State University Digital Repository. For more information, please contact digirep@iastate.edu.

Developing green processes for the conversion of biobased materials into pyrones

by

William Bradley

A dissertation submitted to the graduate faculty

in partial fulfillment of the requirements for the degree of

DOCTOR OF PHILOSOPHY

Major: Chemistry

Program of Study Committee:
George Kraus, Co-major Professor
Eric Cochran Co-major Professor
Levi Stanley
Arthur Winter
Javier Vela-Becerra

The student author, whose presentation of the scholarship herein was approved by the program of study committee, is solely responsible for the content of this dissertation. The Graduate College will ensure this dissertation is globally accessible and will not permit alterations after a degree is conferred.

Iowa State University

Ames, Iowa

2019

Copyright © William Bradley, 2019. All rights reserved.

DEDICATION

I dedicate this work to my family.

TABLE OF CONTENTS

NOMENCLATURE	v
ACKNOWLEDGMENTS	vi
ABSTRACT	viii
CHAPTER 1. GENERAL INTRODUCTION AND CORROSION INHIBITORS FROM TRIACETIC ACID LACTONE	1
1.1. Introduction	1
1.1.1. Biomass feed stocks versus petroleum feed stocks	1
1.1.2. Biomass conversion	3
1.1.3. Platform molecules	4
1.1.4. Pyrones in the literature	6
1.1.5. Corrosion inhibitors	8
1.2. Results	10
1.3. Conclusion	15
1.4. Experimental	16
1.4.1. General information	16
1.4.2. Potential electrochemical impedance spectroscopy	16
1.4.3. Potential dynamics measurement	17
1.5. References	21
CHAPTER 2. CONVERTING 1,3-DICARBONYL COMPOUNDS TO γ -PYRONES	23
2.1. Introduction	23
2.1.1. Background of γ -pyrone	23
2.1.1.1. [3+3] Reactions	23
2.2. Results	27
2.3. Conclusion	31
2.4. Experimental	31
2.4.1. General information	31
2.4.2. Agar overlay	38
2.5. References	39
CHAPTER 3. APPLICATIONS OF CITRIC AND MALIC ACID	41
3.1. Introduction	41
3.1.1. Citric acid and malic acid	41
3.1.2. Von Pechmann reaction	41
3.2. Results	42
3.2.1. Diacid pyrone synthesis	42
3.2.2. Plasticizer mixture synthesis	45

3.3.	Conclusion	46
3.4.	Experimental	46
3.4.1.	General information	46
3.4.2.	Differential scanning calorimetry (DSC).....	48
3.5.	References.....	49
CHAPTER 4. BLENDING THE EFFECTIVENESS OF ANIONIC POLYMERIZATION WITH THE VERSITILITY OF RAFT BY USE OF THE ATOM TRANSFER RADICAL ADDITION-FRAGMENTATION TECHNIQUE		50
4.1	Introduction.....	50
4.1.1	Controlled radical polymerization	50
4.1.2	Block-copolymer.....	52
4.2	Results.....	53
4.2.1	Polystyrene end-group modification.....	53
4.2.2.	Di-block copolymer development.....	56
4.2.3	Macromonomers	59
4.3	Conclusion	62
4.4	Experimental.....	63
4.4.1	Polymerization of styrene	63
4.4.2	PS-OH: Hydroxylation of living polystyrene	63
4.4.3.	Silane synthesis ((3-chloropropoxy)trimethylsilane).....	64
4.4.4.	PS-OH-S: silyl capping.....	64
4.4.5.	PS-Br: tert-bromine capping	65
4.4.6.	ARGET ATRAF method	66
4.4.7.	Photocatalyzed, metal free ATRAF.....	67
4.4.8.	PS-Acrylate block copolymers: PS-CTA mediated RAFT polymerization of acrylates	67
4.4.10.	Gel permeation chromatography (GPC)	69
4.4.11.	Nuclear magnetic resonance spectroscopy (1H-NMR)	69
4.4.12.	Differential scanning calorimetry (DSC).....	69
4.4.13.	Transmission electron microscopy (TEM)	69
4.4.14.	Dynamic shear rheology (DSR).....	69
4.5	References.....	75
CHAPTER 5. GENERAL CONCLUSION		78

NOMENCLATURE

Ac	Acetyl
Aq.	Aqueous
TAL	Triacetic Acid Lactone
Ar	Aryl
°C	Degrees centigrade
g	Gram
LDA	Lithium diisopropylamide
CoA	coenzyme A
dd	doublet of doublets
s	Singlet
t	triplet
THF	Tetrahydrofuran
NBS	N-Bromosuccinimide
DMF	N,N-dimethylformamide
Pd/C	Palladium on Carbon
Ph	Phenyl
TBS	Tert-butyldimethylsilyl
TMS	trimethylsilyl
RAFT	Reversible Addition Fragmentation Chain- Transfer

ACKNOWLEDGMENTS

I would like to acknowledge and show gratitude to all the people who have supported me for my time as a graduate student. First, I would like to thank Dr. Kraus for welcoming me into his group as a second-year graduate student, and for his training, guiding and challenging me to become an independent thinking scientist. His passion and mentoring in chemistry have been vital to my growth in creativity, organization, leadership, understanding synthetic fundamentals and methodology development. It is also important to give gratitude to Dr. Cochran for co-advising me and accepting me as an extended member of his group. Learning chemical engineering principles and scale up have been important to my development. Thank you, to every member of Dr. Kraus and Dr. Cochran group for helping me and teaching me throughout my Ph.D. career.

I would like to thank my graduate committee members Dr. Kraus, Dr. Cochran, Dr. Stanley, Dr. Winter, Dr. Woo, and Dr. Vela for taking the time to be a guide throughout the course of my research and time at Iowa State University. Learning about your research and getting to know all of my committee members has been a pleasure.

It is important to acknowledge the help from funding opportunities from the NSF Engineering Research Center for Biorenewable Chemicals CBiRC and the United States Department of Agriculture. At this point, I need to thank Dr. Jason Chen for first accepting me into his group at Iowa State University and starting my funding with the Department of Agriculture grant for the development of bio-based tackifiers. The financial assistance from these entities have been most appreciative for the work enclosed.

I want to also give a special thanks to all of my collaborators that I have had the opportunity work with over the past 6 years. Their collaboration has been essential, and I would

not be here today without all of their support. In the anionic and RAFT block copolymer project, the work completed would have been impossible without Michael Forrester. Thank you, for being my friend, colleague, collaborator, and teaching me about polymer science. I also want to thank Fang-Yi Lin for all of the assistance with the material characterization of the block copolymers. Thank you, Jiajie Hao for teaching me and working with me for the corrosion work, I enjoyed getting to know you and learning about the application of the corrosion inhibitors. I want to thank Allison Brost for testing some of my synthesized molecules for antimicrobial activity and helping me with some last-minute assays.

It is important to thank all the wonderful lab mates that I have worked with. I acknowledge their mentorship and friendship throughout my Ph.D. a thank you to: Huangchao Yu, Yang Qu, Ivan Geraskin, Akbar Khan, Gayan Abeykoon, Michael Zenner, Shreyosree Chatterjee, Fang-Yi Lin, Michael Forrester, Nacu Hernandez, Austin Hohmann, Josh Alterman, Shuai Wang, Kyle Podolak, Aleksei Ananin, Ben Kosieradzki, Kristina Nugent, and Chris Rybak. All of you have been essential for my path to completing this document.

Finally, my family have been essential in my growth for completing my Ph.D. My father, Dr. Steven Bradley for teaching me about the career path of being a chemist. My mother, Janice Bradley, thank you for always listening to me on both my good and bad days, and all my siblings for their support.

ABSTRACT

The work disclosed in this dissertation implements bio-based material for new synthetic applications. The synthetic applications are corrosion inhibitors, plasticizers, and block copolymers. Triacetic Acid Lactone (TAL) is a bio-based molecule fermented from *Saccharomyces cerevisiae*. In the first chapter, we discuss the conversion of triacetic acid lactone to corrosion inhibitors. The synthesis utilizes a nucleophilic heterocycle undergoing conjugate addition with brominated TAL producing a corrosion inhibitor. Successful corrosion inhibitors were synthesized in moderate to good yields. The highest corrosion inhibitor efficiency was 88% for newly developed corrosion inhibitors.

In the second chapter we developed a methodology to generate γ -pyrones. This moiety was formed by a [3+3] reaction between a 1,3 dicarbonyl and dihaloacryloyl chloride. Bicyclic γ -pyrones could be transformed into 5-hydroxychromones by aromatization in good yields.

In the third chapter, we found new applications for citric and malic acid mixtures (similar to those found in fruit) by converting them into plasticizers. Citric and malic acid could be reacted together to form an α -pyrone diacid in 76% yield. The reaction was conducted in concentrated sulfuric acid. The esters of citric and malic acid could also be reacted together to afford the diester pyrone.

In the fourth chapter, we combined anionic polymerization with reversible addition fragmentation chain transfer RAFT polymerization by the development of macro-chain transfer agent. The conversion of anionic polystyrene to block acrylic copolymers had an efficiency as high as 97%. This was completed by coupling α -bromoisobutryl bromide, followed by atom-transfer radical addition fragmentation transfer with bis(thiobenzyl)disulfide to add the chain

transfer agent functionality. The methodology of combining anionic polymerization with RAFT polymerization gave the highest blocking efficiency known in the literature.

CHAPTER 1. GENERAL INTRODUCTION AND CORROSION INHIBITORS FROM TRIACETIC ACID LACTONE

William Bradley, Jiajie Hao, Brett Shanks, George Kraus

1.1. Introduction

There are a wide variety of non-renewable fossil fuel derived materials used in society such as plastics, dyes, surfactants, plasticizers, corrosion inhibitors, tackifiers, and pharmaceuticals. These fossil resources may be fiscally inexpensive yet are not sustainable due to the inability to replenish the resources. Most materials come from a limited supply of coal, natural gas, and crude oil. Furthermore, petroleum only exists in specific locations, causing volatile price changes as the world economy changes. Renewable resources for energy production are geothermal, solar, biofuels, tidal and wind. While there is a lot of effort to convert renewable resources into energy, the decrease on dependency on fossil resources will require the design of new renewable materials. Renewable materials are not directly affected by the volatile costs of fossil fuels. Chemicals derived from fossil fuels will need to be replaced as society moves away from fossil fuels.

1.1.1. Biomass feed stocks versus petroleum feed stocks

Coal, natural gas, and crude oil have supplied the fossil fuel industry since the beginning of the industrial revolution. In organic chemistry the olefin and aromatic products from crude oil have been developed into a number of highly applicable molecules. The petroleum feedstock propylene can be transformed into a number of different molecules (Figure 1.1). Isopropyl alcohol is a commonly used organic solvent and used as rubbing alcohol to clean wounds. Acrylates have synthetic applications; one such example uses Diels Alder reactions with furan to form methyl benzoate.¹ Acrylates are also used in the development of polymers.

These acrylate polymers have a number of different applications such as: acrylic paints, viscosity modifiers, and pressure sensitive adhesives.

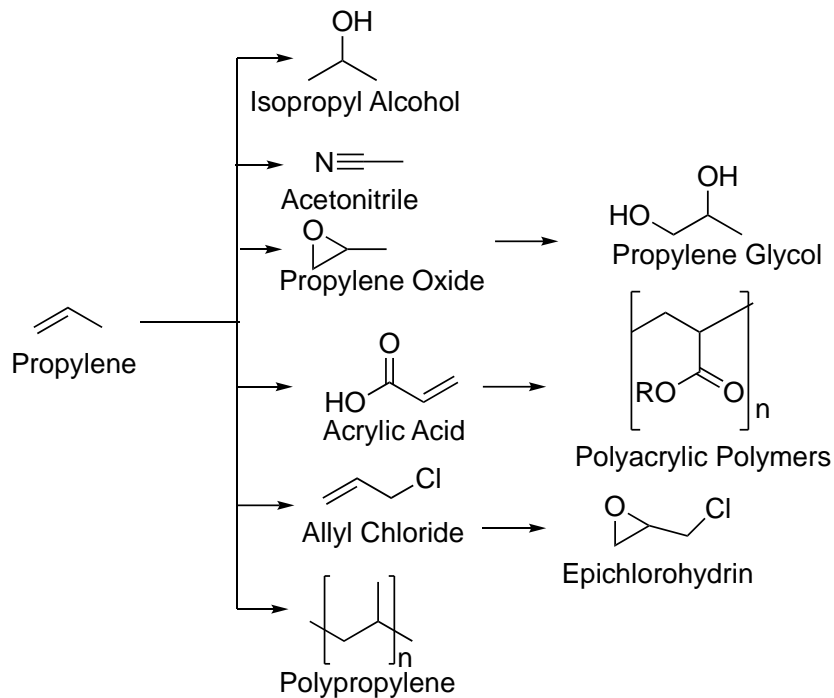


Figure 1.1. Products from Propylene

While acrylates historically are developed from petroleum sources, in the past few years, an effective route has been uncovered using glycerol as a feed stock.² Glycerol is a triol that is a bio-based molecule that can be isolated from plants. However, competing directly with petroleum feedstock molecules is difficult and even more difficult to match on a fiscal basis. There are pressing environmental reasons to use bio-based feed stocks to replace petroleum feed stocks. Instead of just making drop-replacements, another use of bio-based feed stock is to transform the feed stocks into novel chemicals with advantageous properties. These novel molecules increase the opportunities for new applications.

1.1.2. Biomass conversion

Biomass exists in different forms. There are bacteria, animals and plants producing this feedstock. Globally, biomass production can be found in 60% terrestrial origin and 40% aquatic origin. Out of the biomass that is cultivated, 75% comes from carbohydrates, 20% from lignin, and 5% from the remaining groups (Figure 1.2).³

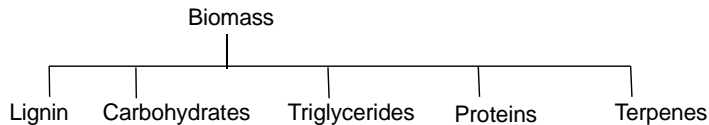


Figure 1.2. Major Categories of biomass³

Lignin and cellulose are advantageous biopolymers because they are not edible by humans. These biomass materials can be converted into many organic molecules by thermochemical or biological conversions. Thermochemical conversions use heat and pressure to convert the biomass to useful organic molecules. For example, in pyrolysis, this technique uses heat to decompose the organic biomass into more useful organic molecules. Another example is to use liquefaction. This decomposes the biomass by using heat and pressure to do the decomposition.

In biological conversions of biomass, microbes use fermentation and anaerobic respiration to convert the raw biomass into applicable organic molecules. Fermentation is a process where the biomass is converted to materials along the microbes' anaerobic pathway. In this process the biomass is converted into methane, hydrogen gas and organic compounds. Between biological and thermochemical conversions, it is possible to convert biomass into biofuels and chemicals.⁴

1.1.3. Platform molecules

Biomass can be converted into platform molecules that can be converted into identical petroleum chemicals or new chemicals. At the end of the 20th century, biobased feed stocks have been converted into bio-based platform molecules to generate chemicals and materials.^{5,6} In Figure 1.3 there are examples of platform chemicals that can be converted into more expensive end products.⁷

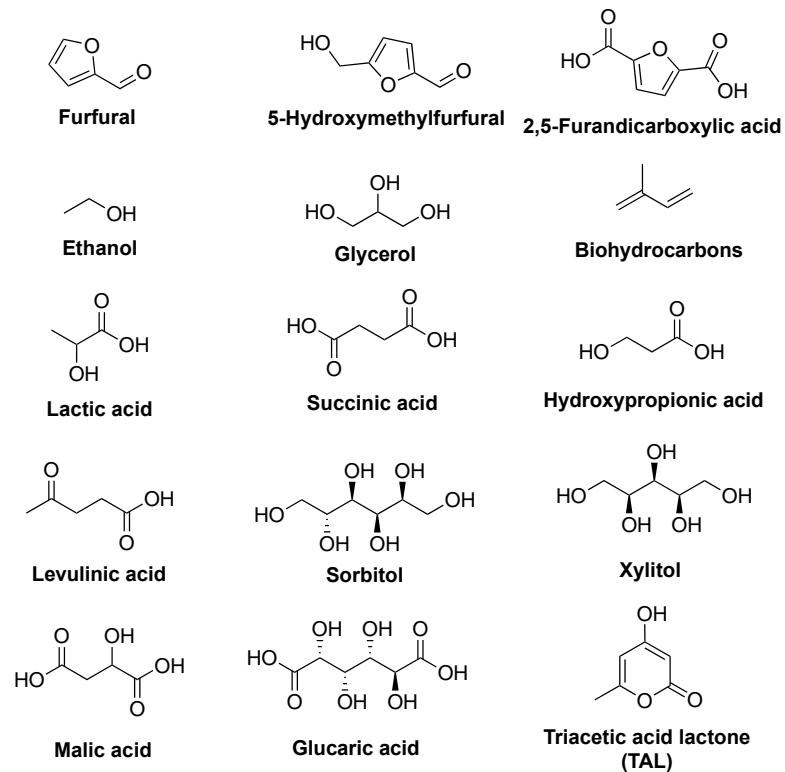


Figure 1.3. Bio-based Platform molecules

One such bio-based platform molecule incorporated is malic acid, a chemical which can be converted into a variety of products (Figure 1.4). Recently, malic acid can be produced from *Aureobasidium pullulans* a fungus that can produce polymalic acid.⁸ Polymalic acid can be cleaved by hydrolysis of the polyester to produce malic acid. Malic acid is a product of the citric acid cycle metabolic pathway and many organisms have produced malic acid. Fruit such as

apples attribute 94% of the acidity content to malic acid.⁹ Malic acid can be converted by reduction using BH_3 to 1,2,4-butanetriol.¹⁰ This compound can be used for the development of alkyds, additives for coating production. Maleic acid can be produced from malic acid by dehydration of the alcohol. This acid can also be dehydrated further to produce maleic anhydride, a useful compound for polymerization. Isomerization of maleic acid by photolysis with Br_2 would convert the cis acid into the trans fumaric acid. Dimerization of decarbonylated malic acid forms coumalic acid in strong acidic conditions, an acid that is valued because of its rigid pyrone moiety. Coumalic acid can undergo Diels Alder reactions to form isophthalic acid as well as trimellitic anhydride.¹¹ These bio-based products are the same as ones produced from petroleum-based products and are useful. The different products of malic acid, as shown above, were the reason in 2015 the DOE marked malic acid as a top bio-based molecule.¹² While malic acid is an efficient bio-based platform molecule, it is necessary to explore other avenues to incorporate more bio-based molecules in society's infrastructure.

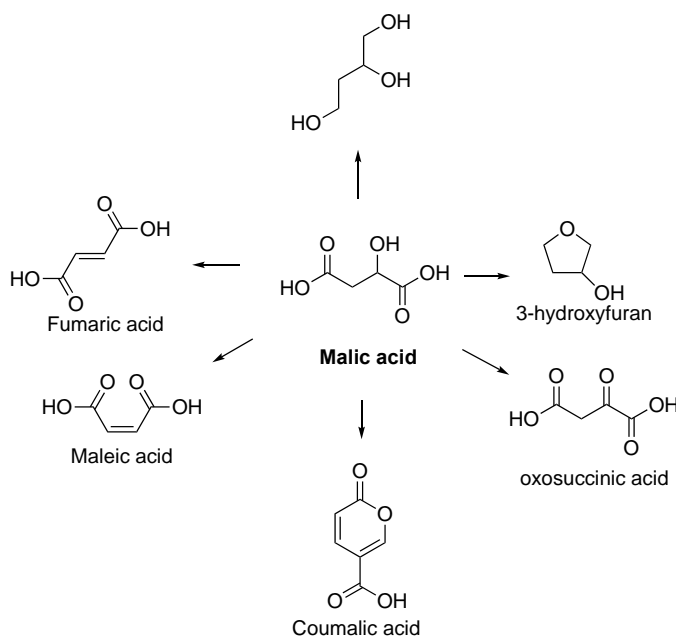


Figure 1.4. Malic Acid as a platform molecule.

1.1.4. Pyrones in the literature

One bio-based platformed molecule is triacetic acid lactone (TAL), which has a pyrone functional group. The pyrones are a class of molecules with 6-membered rings and contains a carbonyl with an oxygen that is in an aromatic ring. In this class of molecules there are two isomers. The 2-pyrone is a molecule with a lactone (Figure 1.5). The 4-pyrone has an oxygen in the 4 position of the ring (Figure 1.5). In these 4-pyrones the oxygen still in conjugation with the carbonyl group.^{1,2} These molecules tend to be stable and can be converted into bioactive molecules and have unique material properties. Many pyrones are in the secondary metabolite class known as polyketides.

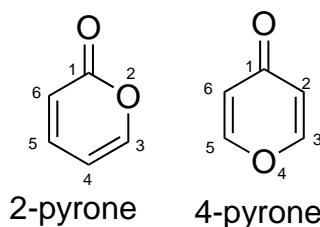


Figure 1.5. Structure of 2-pyrones and 4-pyrones

Pyrones are highly abundant in various different structures from biology. An example of 2-pyrone biosynthesis is the synthesis of triacetic acid lactone (TAL). TAL is the fermentation product from *Escherichia coli* and *Saccharomyces cerevisiae* by the addition of 6-methylsalicylic acid synthase gene. This gene is isolated from *Gerbera hybrida*. The gene that is responsible for the production of α -pyrone synthase. These bacteria utilize the enzyme 2-pyrone synthase with acetyl-CoA and malonyl-CoA.³ TAL has been found to have negative effects on *E. coli*, and showed a reduction in growth rate of 25% and 90% in 10mM and 20mM TAL, respectively.¹³ Toxicity is lower for *Saccaromyces cerevisiae*, and the microbe is not effected by 200 mM TAL.

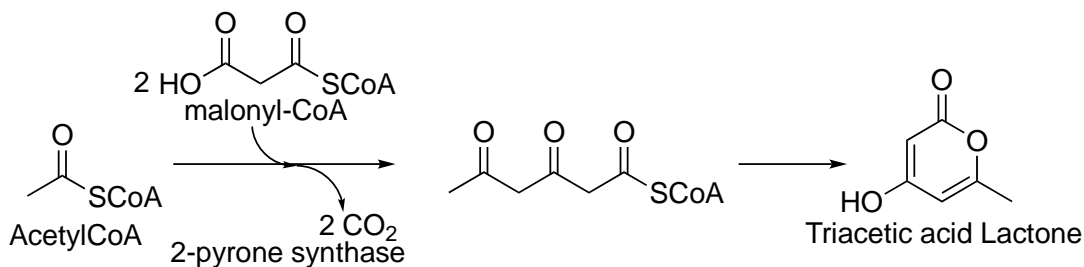


Figure 1.6. Biosynthetic pathway in *Saccharmyces cerevisiae*.

There are natural products with α -pyrone moieties, some shown in Figure 1.7. From the fungus *Stereocaulon tomentosum*, the cytotoxic dothideopyrone F was recently discovered in 2018 by Ahn.⁸ This bio active pyrone showed the ability to decrease mRNA expression levels of tumor necrosis factor α (TNF- α) in mice. As dothideopyrone F inhibits the nitric oxide production, causing the cell to become less likely to mutate. In other bioactive α -pyrones 6-pentyl-2-pyrone (Figure 1.7) has shown inhibitory effects against pathogenic fungi: *Aspergillus*, *Botrytris*, *Rhizoctonia*, *Sclerotinia*, and *Pyrenochaeta*.⁹

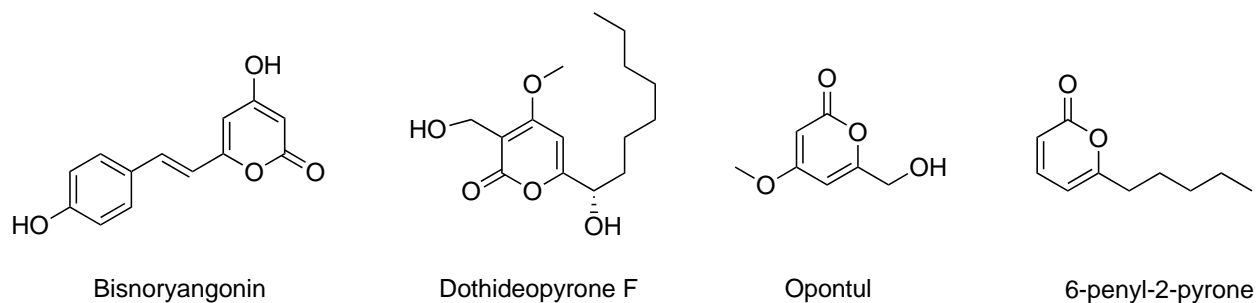


Figure 1.7. 2-Pyrone natural products.

Triacetic acid Lactone (TAL) is a platform green chemical. In the Kraus laboratory, TAL was transformed into pogostone in one step.¹⁴ In this synthesis Kraus developed 6 analogs from TAL. Pogostone is an insecticide that was found effective against *Myzus persicae*. Xian found that against *Myzus persicae*, pogostone had a repellency index of $0.230 \pm 0.07aA$ at a concentration of 125 mg/L over the course of 24 hours.¹⁵

In 2018, Obydenov developed a method of converting TAL into azaheterocycles. These heterocycles (Figure 1.8) have been found to have biological activity. The synthesis consists of adding two equivalents of a primary amine followed by the addition of hydrazine to form the azaheterocycle.

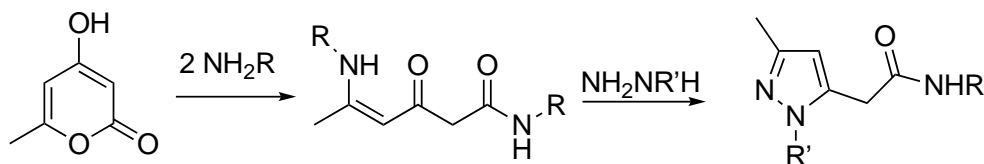


Figure 1.8. Synthetic applications of TAL to azaheterocycles

1.1.5. Corrosion inhibitors

Corrosion inhibitors are additives that decrease the rate of corrosion of a metal or an alloy. For example, in a number of water pipes, small amounts of acid corrode pipes overtime. These acids corrode the pipes and can deposit iron oxides or rust, lowering stability of the alloy. In oil fields a number of iron pipes corrode and become damaged over time due to a minor amount of acid in the facility. According to Fingar, developing more efficient corrosion inhibitors for acidic, oxygen rich, and high temperature conditions are valuable for increasing chemical durability.¹⁶

The mechanism of action of corrosion inhibitors can be divided into three categories. Anodic corrosion inhibitors are a type of corrosion inhibitors that are inorganic. These anodic corrosion inhibitors' mechanism of action surrounds the metal with hydroxide anions.¹⁷ This prevents acid from reacting with the metal. Examples of anodic corrosion inhibitors include KMnO_4 , Na_2CrO_4 , K_3PO_4 , and NaNO_3 . Issues with anodic corrosion inhibitors are the threshold requirements of the inhibitors. If concentrations are too low, the inhibitor will not fully cover the metal and accelerate the corrosion in acidic conditions.¹⁸

Cathodic corrosion inhibitors are another example of inorganic corrosion inhibitors. These inhibitors' mechanism of action utilizes inexpensive metals to react with electrolyte media to produce insoluble salt that with surrounds the metal.¹⁸ Major issues with cathodic corrosion inhibitors are the loss of conductivity in the metal being protected and salt residue cover the surface of the metal. Examples of cathodic corrosion inhibitors include magnesium, nickel, and zinc.

The final category are adsorption corrosion inhibitors, which fall in the category of organic corrosion inhibitors. This work is on developing new adsorption corrosion inhibitors. Adsorption corrosion inhibitors chelate to the metal or are coated on to the metal surface. Polymers such as polyethylene oxide are coated to the metal, stopping water and electrolytes from interacting with the metal surface. Adsorption corrosion inhibitors that chelate to the metal are small molecules that surround the metal in a single layer coating, which slows the metal from interacting with the electrolyte solution. Some example of adsorption organic corrosion inhibitors include 2-mercaptopyridine, 4-mercaptopyridine, cystine, and histidine.¹⁹ Structural aspects that affect a molecule's ability to coordinate to the metal surface include: heteroatoms such as phosphorus, sulfur, and nitrogen, aromatic functionality, and hydrophobic groups.¹⁹ The organic corrosion inhibitors must also be water soluble.

Known organic corrosion inhibitors, 2-mercaptopyridines and 4-mercaptopyridines (Figure 1.9.) have been tested with gold metal and iron metal with an electrochemical impedance spectroscopy test.²⁰ In the work it was shown by measuring the impedance of the corrosion by measuring the resistance on the metal anode. The corrosion inhibitors showed an impedance of 63% and 58% for 2-mercaptopyridine and 4-mercaptopyridine, respectively, for the iron anode.

These organic corrosion inhibitors chelate with the metal to form self-assembled monolayer coatings around the metal preventing the corrosion.

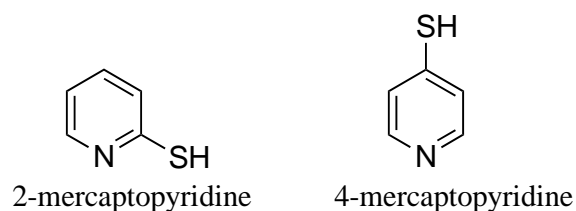
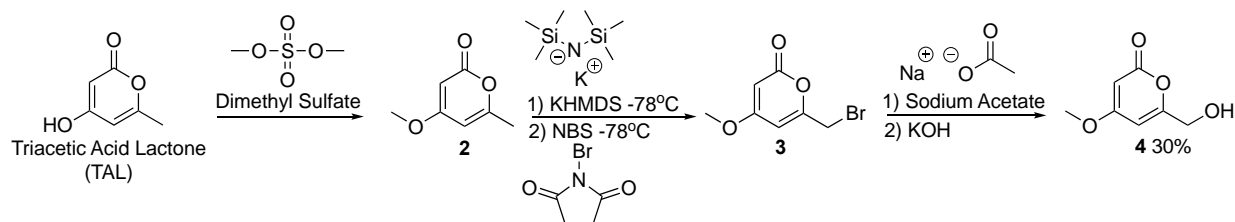


Figure 1.9. Known corrosion inhibitors for iron and gold.

The testing of organic corrosion inhibitors would utilize electrochemical impedance spectroscopy. This test measures the amount of corrosion by measuring the resistance from the mild steel plating.

1.2. Results

It was initially reported opuntiol was found to be an effective corrosion inhibitor.²⁰ Opuntiol was synthesized in 30% overall yield as shown in Figure 6, using triacetic acid lactone (TAL) as a starting material. TAL was methylated with dimethyl sulfate to synthesize **2**. The methylated TAL was the deprotonated with KHMDS followed by NBS synthesizing **3**. An anionic route was used for synthesis of **3** due to lack of regioselectivity from radical bromination. Finally, **3** was converted to **4** (opuntiol) with a substitution and saponification. Opuntiol was found by our studies to be a poor corrosion inhibitor as seen in Table 1.1.



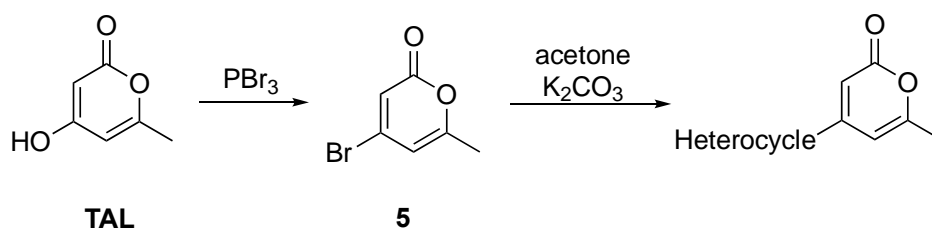
Scheme 1.1. Synthesis of Opuntiol

Table 1.1. Replicated Opuntiol corrosion efficiency.

Conditions	[Opuntiol]	Inhibitor Efficiency
0.3 M HCl	156 ppm	15%
0.1 M H ₂ SO ₄	156 ppm	13%

New corrosion inhibitors were developed based on TAL, since Opuntiol was not an effective corrosion inhibitor in acidic media. These corrosion inhibitors required different heteroatoms other than oxygen to coordinate the mild steel alloy. Each synthesized corrosion inhibitor would be compared to urotropine, a commercially used organic corrosion inhibitor.

Development of the various corrosion inhibitors utilized triacetic acid lactone and PBr₃ to substitute the hydroxyl group for the bromine (Scheme 1.2). The synthesis of **6a-6g** were produced in good yields by introducing a nucleophilic heterocycle. However, nitrogen nucleophiles were unable to produce **6h** and **6i** were unable to be converted to products.



Scheme 1.2. Synthesis of corrosion inhibitors

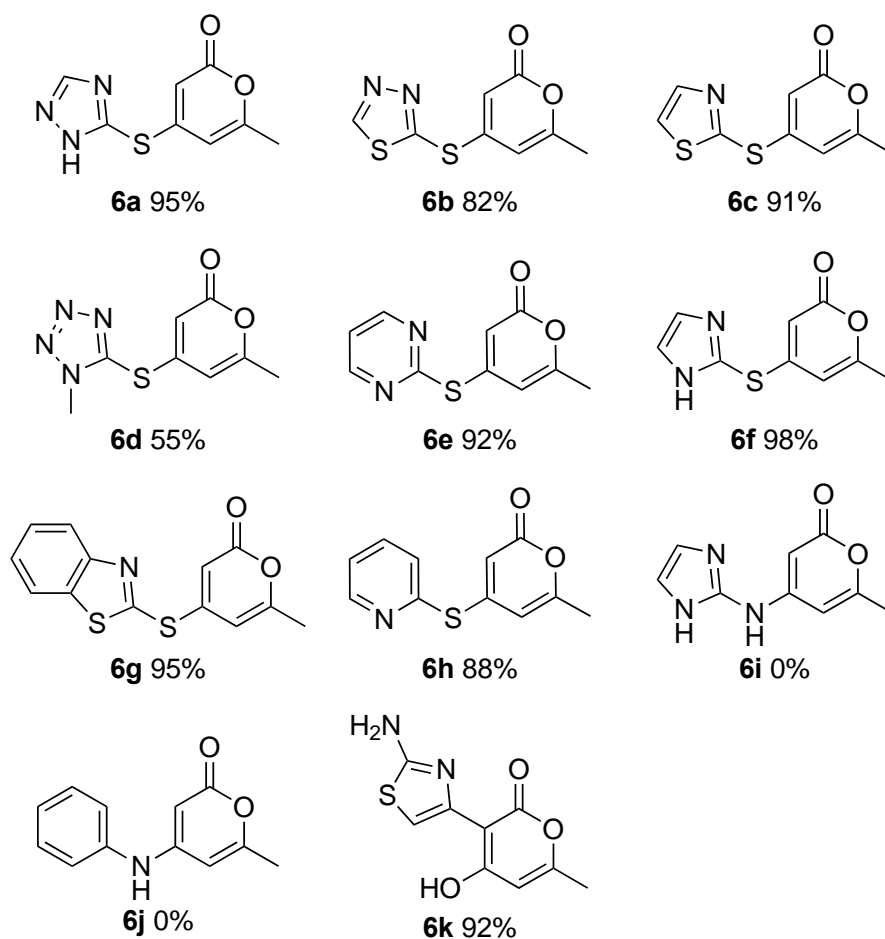


Figure 1.10. Corrosion inhibitor yields

Each corrosion inhibitor was then tested and compared with the corresponding starting material heterocycle as well as the standard urotropine for the ability to impede corrosion of a 0.1M HCl electrolyte as shown in Table 1.2. Each 0.1M HCl solution had 1mM corrosion inhibitor added. Urotropine showed a corrosion inhibitor efficiency of 40% and was tested each time before the electrochemical impedance spectroscopy was used. TAL without any additional substituents showed 0% corrosion inhibitor efficiency. Corrosion inhibitor **6a** displayed a corrosion inhibitor efficiency of 88%, the heterocycle base had a corrosion inhibitor efficiency of 37%. The combination of the heterocycle base with TAL in the **6a-c** corrosion inhibitor demonstrated an increase in corrosion inhibitor efficiency in comparison to the sum of the parts.

Not all corrosion inhibitors **6a-6k** showed a corrosion inhibitor efficiency. Corrosion inhibitors **6e** and **6f** decreased the corrosion inhibitor efficiency when compared with the heterocyclic base. A known corrosion inhibitor heterocycle base, 2-thiolbenzothiazole showed 88% corrosion inhibitor efficiency. The corrosion inhibitor efficiency of bezothiazole-2-thiol remained an effective corrosion inhibitor at 88% when it was added to TAL. Both **6k** and thiourea were found to be poor corrosion inhibitors based on the 28% corrosion inhibitor efficiency. All negative corrosion inhibitor values indicate an acceleration of corrosion. All increases or decreases of corrosion inhibitor efficiency are hypothesized to be the organic corrosion inhibitor's ability to bind to the mild steel as a single layer coating.

Table 1.2. Corrosion Inhibitor efficiency of in 0.1M HCl + 1 mM inhibitor

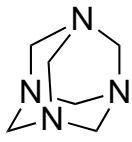
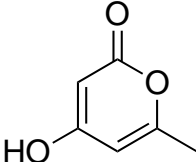
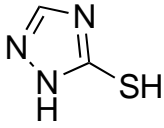
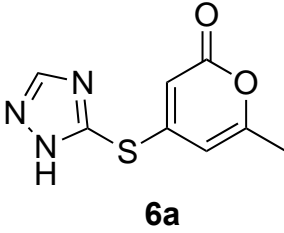
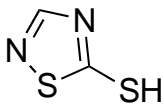
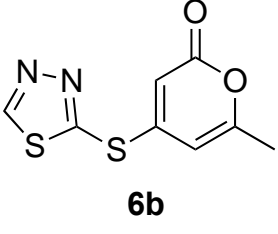
Corrosion Inhibitor Standard	Corrosion Inhibitor Efficiency	Triacetic acid Lactone	Corrosion Inhibitor Efficiency
 Urotropine	40%		0%
	37%	 6a	88%
	-54%	 6b	65%

Table 1.2. (continued).

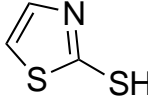
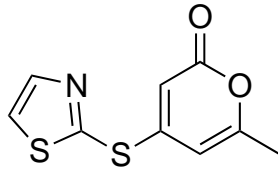
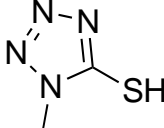
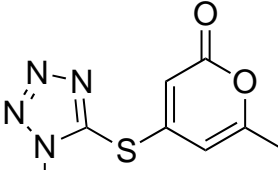
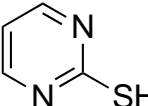
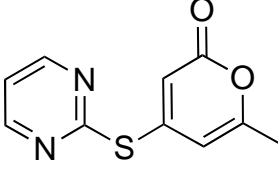
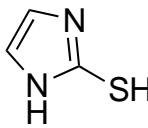
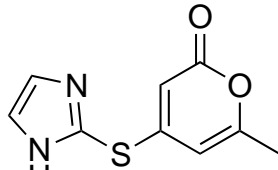
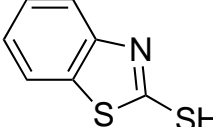
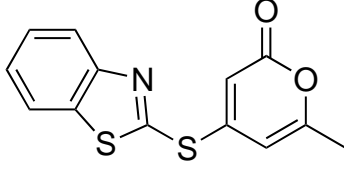
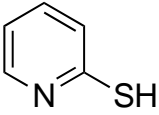
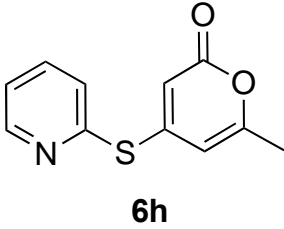
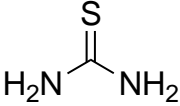
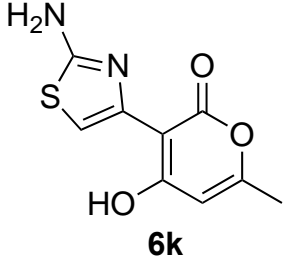
	41%	 6c	73%
	-300%	 6d	-42%
	73%	 6e	2%
	41%	 6f	2%
	88%	 6g	88%

Table 1.2. (continued).

	72%	 6h	69%
	0%	 6k	28%

1.3. Conclusion

In chapter 1 we have developed new applications for the platform molecule TAL. The utilization of TAL to increase corrosion inhibitor efficiency of a heterocyclic base is an example of biorenewable enhancement, in a 2-step approach. While this work does not remove all petroleum mass from the corrosion inhibitors, it does add ~50% biorenewable mass to the corrosion inhibitors. Work will continue, on the corrosion inhibitor development. Not all corrosion inhibitors tested were successful; however, and this point brings future research questions. Determining the mechanism of action of these corrosion inhibitors is necessary. In order to determine the mechanism, it will be necessary to incorporate computational studies to complete this task. Understanding the mechanism would allow prediction of what allows an organic molecule to be an effective corrosion inhibitor.

1.4. Experimental

1.4.1. General information

All starting materials were purchased from Sigma-Aldrich, AK Scientific Institution and Oakwood Chemical; Solvents were all purchased from Sigma-Aldrich and Fisher Scientific and used without further distillation. All reactions were monitored by thin layer chromatography (TLC) and ^1H NMR. All yields refer to separated yield after column chromatography unless indicated. TLC was obtained by silica plate using UV light as a visualizing agent or Potassium permanganate solution with heat. All columns were performed with silica gel 60 Å, particle size 40-63 μm . ^1H and ^{13}C NMR spectra were acquired in CDCl_3 or other deuterated solvents on a Varian MR-400 or Bruker Avance III 600 MHz spectrometer.

1.4.2. Potential electrochemical impedance spectroscopy

See the figure below, a VSP-300 Potentiostat from Bio-logic with EC-LAB software was used for the PEIS test. The test was performed in a conventional 3-electrode cell with a Ag/AgCl reference electrode, a Pt coil counter electrode and a working electrode. Polished mild steel before and after the test was added in the figure below.

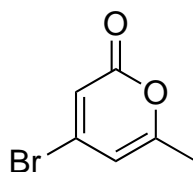


Figure 1.11. Electrochemical Impedance Spectroscopy

1 L of 0.1 M sulfuric acid or 0.3M hydrochloric acid was prepared using nanopure water. Fresh 3 mM of hexamethylenetetramine (urotropin) in 0.1 M sulfuric acid solution was prepared before each test. Mild steel A366/1008 (from Onlinemetals.com) was cut into 1 cm*3 cm coupon. The steel was manually polished with 600, 800, 1200, and 2000 grade silica carbide sanding papers, then rinsed with ethanol and sonicated for 3 minutes. After wiped with Kimwipe, the steel coupon was wrapped in the center to ensure that exposed end surface area was 1 cm². A Bio-logic VSP300 was used for the test. Aliquot of 40 mL of 0.1 M sulfuric acid with or without hexamethylenetetramine was added into the cell, which was then put in a 30 °C water bath on a heating plate. An open circuit voltage was recorded and stabilized for 30 min. Electrochemical impedance measurements were performed at the open circuit voltage. Frequency ranged from 10⁵ to 10⁻³ Hz with an amplitude of 10 mV was used for the test. After the analysis, the built-in software was used to do the Z-fit of Randles equivalent circuit to obtain charge transfer resistance. Based on the charge transfer resistance, the inhibition efficiency was calculated.

1.4.3. Potential dynamics measurement

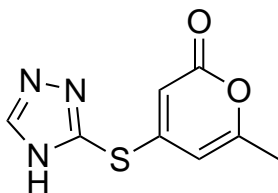
For the potential dynamic measurement, the Tafel plot was obtained after the 30 min of open circuit voltage. The potential was scanned from OCV-300 mV to OCV+300 MmV with a 0.5 mV s⁻¹ sweep rate.



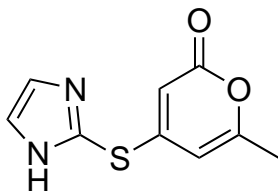
Synthesis of 5. To a 10 mL DMF solution at 0°C. was added dropwise a solution of 32 mmol PBr₃ in 18 mL of distilled diethyl ether. Then, 8.0 mmol pyrone solution in 8 mL DMF was transferred to the PBr₃ solution via cannula. The resulting mixture was heated to 60°C. for

overnight. The reaction mixture was subsequently cooled to 0°C., then quenched with 40 mL of distilled water, and extracted with 6 x 20 mL of ethyl ether. The combined ethyl layer was washed with 50 mL of distilled water, dried over MgSO₄, and concentrated to give **5**, yield 80%
¹H NMR (400 MHz, Chloroform-d) δ 6.46 (d, J = 1.7 Hz, 1H), 6.19 (d, J = 1.7 Hz, 1H), 2.25 (s, 3H). MS = 187 M/Z

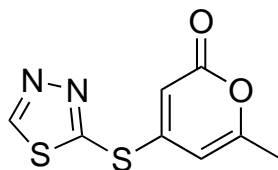
Synthesis of 6a-6h. 1mmol **5** was added to a round bottom flask with 5 mmol Na₂ CO₃, 5 mL of acetone, and 1.1 mmol of a corresponding heterocycle. The mixture was stirred at room temperature overnight. The reaction was monitored by TLC and was filtered to remove Na₂CO₃, and washed with acetone. Solvent was then removed with reduced pressure and a yellow solid formed. The solid would be passed through silica column with ethyl acetate mobile phase. Further purification was performed by trituration with n-hexanes.



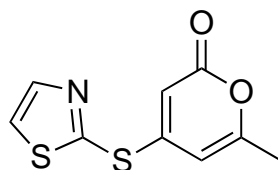
¹H NMR (400 MHz, DMSO-d₆) δ 8.80 (s, 1H), 6.19 (s, 1H), 5.74 (d, J = 1.7 Hz, 1H), 2.17 (s, 3H). MS 209 M/Z



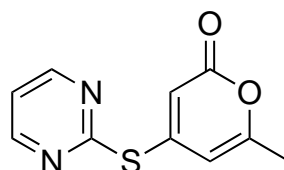
¹H NMR (400 MHz, DMSO-d₆) δ 7.23 (s, 2H), 6.05 (dd, J = 1.9, 1.0 Hz, 1H), 5.37 (dd, J = 1.7, 0.7 Hz, 1H), 2.15 (s, 3H). MS 208 M/Z



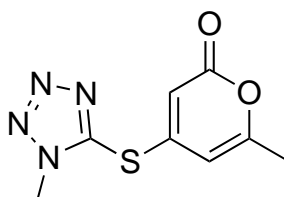
¹H NMR (400 MHz, DMSO-d₆) δ 9.90 (s, 1H), 6.32 – 6.26 (m, 1H), 5.93 (t, J = 1.2 Hz, 1H), 2.19 (s, 3H). MS 225 M/Z



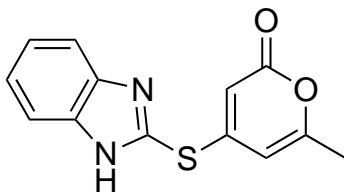
¹H NMR (400 MHz, DMSO-d₆) δ 8.19 – 8.11 (m, 2H), 6.22 (dd, J = 1.8, 1.0 Hz, 1H), 5.69 – 5.64 (m, 1H), 2.19 – 2.17 (m, 3H). MS 224 M/Z



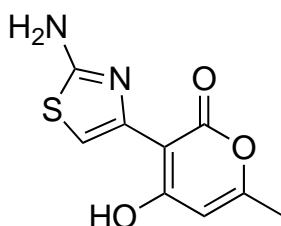
¹H NMR (400 MHz, DMSO-d₆) δ 8.79 (d, J = 4.9 Hz, 2H), 7.45 (t, J = 4.9 Hz, 1H), 6.72 (d, J = 1.5 Hz, 1H), 6.43 (s, 1H), 2.21 (s, 3H). MS 220 M/Z



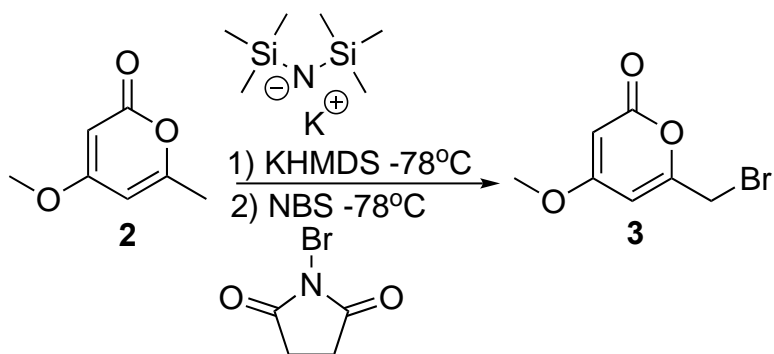
¹H NMR (400 MHz, DMSO-d₆) δ 6.23 – 6.20 (m, 1H), 5.86 – 5.82 (m, 1H), 4.07 (s, J = 1.1 Hz, 3H), 2.20 – 2.16 (m, 3H). MS 224 M/Z



$^1\text{H NMR}$ (400 MHz, DMSO-d_6) δ 7.52 (dd, $J = 6.2, 3.3$ Hz, 2H), 7.09 (dd, $J = 6.2, 3.3$ Hz, 2H), 6.22 (s, 1H), 6.03 (s, 1H), 2.17 (s, 3H). MS 258 M/Z

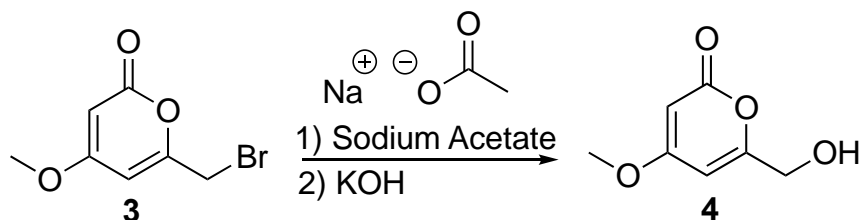


$^1\text{H NMR}$ (400 MHz, DMSO-d_6) δ 8.35 (s, 2H), 7.12 (s, 1H), 6.15 (d, $J = 1.1$ Hz, 1H), 2.22 – 2.18 (m, 3H). MS 224 M/Z



Synthesis of 3: Ten mmol of **2** was added to a 500 mL round bottom flask with 80 mL of dry THF. To the mixture 15 mL of 1 M KHMDS was added dropwise over the course of 10 minutes at -78 °C. The reaction was kept at -78 °C for 1 hour, then 15 mmol of NBS dissolved in 50 mL of dry THF was added at -78 °C to the reaction mixture, and was stirred for 1 hour. The mixture was then quenched with 10 mL of saturated ammonium chloride mixture and further diluted with 200 mL H_2O . The reaction mixture was extracted with 3 x 100 mL ethyl acetate and concentrated in vacuo. The yellow oil was then purified with column chromatography. Isolation

of a yellow solid in 60% yield $^1\text{H NMR}$ (400 MHz, Chloroform- d) δ 6.07 (d, $J = 2.2$ Hz, 1H), 5.48 (d, $J = 2.2$ Hz, 1H), 4.09 (s, 2H), 3.80 (s, 3H).



Synthesis of 4: One mmol of **3** was added to a 25 mL round bottom with 1.1 mmol of sodium acetate and 10 mL of ethanol. The mixture was heated to reflux and was stirred for 24 hours. The mixture was cooled to room temperature, then 10 mL of 1 M sodium methoxide was added to the mixture. The reaction was heated to 50 °C overnight. The reaction was then cooled to room temperature, diluted with 40 mL of water and extracted with 5 x 30 mL of ethyl acetate. Solvent was then removed at lowered pressure to yield a yellow solid. The isolated yellow solid in 50% yield. $^1\text{H NMR}$ (400 MHz, DMSO- d_6) δ 6.10 (dd, $J = 2.5, 1.2$ Hz, 1H), 5.63 (t, $J = 6.2$ Hz, 1H), 5.55 (d, $J = 2.3$ Hz, 1H), 4.19 (d, $J = 5.4$ Hz, 2H), 3.80 (s, 3H).

1.5. References

- [1] Mahmoud, E.; Yu, J.; Gorte, R. J.; Lobo, R.F.; *ACS Catalysis* **2015**, 5(11), 6946-6955.
- [2] Kim, M.; Lee, H.; *ACS Sustainable Chemistry & Engineering* **2017**, 5, 11371-11376.
- [3] Sheldon, R. A. *Green Chem* **2014**, 16, 950–963.
- [4] Clark, J.; Deswarte, F. *Introduction to Chemicals from Biomass*; **2015**; pp. 1-309
- [5] Levy, P. F.; Sanderson, J. E.; Kispert, R. G.; Wise, D. L. *Enzyme and microbial Technology* **1981**, 3, 207-215.
- [6] Lipinsky, E. S. *Science* **1978**, 199, 644-651.
- [7] Bozell, J. J.; Petersen, G. R. *Green Chem.* **2010**, 12, 539-554.

- [8] Cao, W.; Wang, Y.; Shen, F.; Luo, J.; Yin, J.; Qiao, C. Wan, Y. *Bioresource Technology* **2019**, 288, 121497.
- [9] Clijsters, H. *Physiologia Plantarum* **1965**, 18(1) 85-94.
- [10] Erickson, L. W.; Lucas, E. L.; Tollefson, E. J.; Jarvo, E. R. *J. Am. Chem. Soc.* **2016**, 138, 42, 14006-14011.
- [11] Kraus, G. A.; Pollock III, G. R.; Beck, C. L.; Palmer, K.; Winter, A. H. *RSC Advances* **2013**, 3(31) 12721-12725.
- [12] Lane, J. BioFuels Digest 2015. The DOE's 12 Top Biobased Molecules.
- [13] Cardenas, J.; Da Silva, N. A. *Metab. Eng.* **2014**, 25, 194-203.
- [14] Yu, J.; Landburg, J.; Shavarebi, F.; Bilanchone, V.; Okerlund, A.; Wanninayake, U.; Zhao, L.; Kraus, G. A.; Sandmeyer, S.; *Biotechnology and Bioengineering* **2018**, 115, 2383-2388.
- [15] Chen, Y.; Li, Y.; Su, Z.; Xian, J.; *BioOne Complete* **2017**, 100(2), 346-349.
- [16] Finsgar, M.; Jackson, J.; *Corrosion Science* **2014**, 86, 17-41.
- [17] Dariva, C. G.; Galio, A. F.; Corrosion Inhibitors- Principles, Mechanism and Applications, Ch. 16.'
- [18] Dariva, C. G.; Galio, A. F.; Corrosion Inhibitors- Principles, Mechanism and Applications, Ch. 16.
- [19] Finsgar, M.; Jackson, J.; *Corrosion Science* **2014**, 86, 17-24.
- [20] Loganayagi, C.; Kamal, C.; Sethuraman, M. G. *ACS Sustainable Chemical & Engineering* **2014**, 2(4), 606-613.

CHAPTER 2. CONVERTING 1,3-DICARBONYL COMPOUNDS TO γ -PYRONES

William Bradley, Allison Brost, Chris Ryback, Dr. Brehm-Stecher, Dr. Kraus

2.1. Introduction

2.1.1 Background of γ -pyrone

A γ -pyrone differs from an α -pyrone in that the oxygen atom of the γ -pyrone is not connected directly to the carbonyl group. These two heterocycles have different biosynthetic pathways.¹ An example of γ -pyrone biosynthesis is kojic acid. Kojic acid is the fermentation product from *Aspergillus oryzae*.² Natural products containing γ -pyrones were first discovered in 1805. An example of a γ -pyrone natural product is Candelalide, (Figure 2.1) which was first isolated in 1966 from the plant pathogenic fungus *Colletotrichum capsica*.³ In rats, this natural product was found to have an LD₅₀ of 16 mg/kg and inhibited mitochondrial respiration.⁴

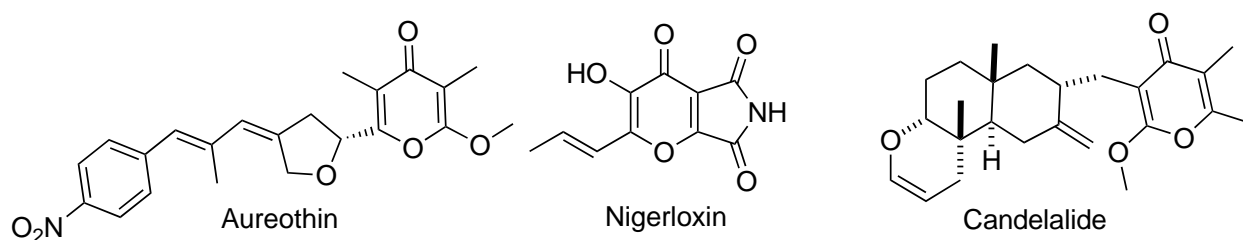


Figure 2.1. 4-Pyrone natural products

2.1.1. [3+3] Reactions

In the synthesis of natural products and other γ -pyrone compounds, a [3+3] cycloaddition reaction can be useful to synthesize these types of compounds. This reaction requires two sets of nucleophiles and electrophiles, one set for the 1,2 addition, and a second nucleophile to react with the second electrophile for the conjugate addition. It has been noted that TAL can be used as the keto-ester moiety to develop a bicyclic compound (Figure 2.2). In the cycloaddition reaction the carbon 3 of the pyrone reacts in a 1,2 addition with the iminium salt. The tertiary

amine then undergoes beta-elimination. After the formation of the 6π electron system, a ring closure occurs to form the 2-H pyran. This [3+3] ring closure reaction a Knoevenagel condensation.⁵

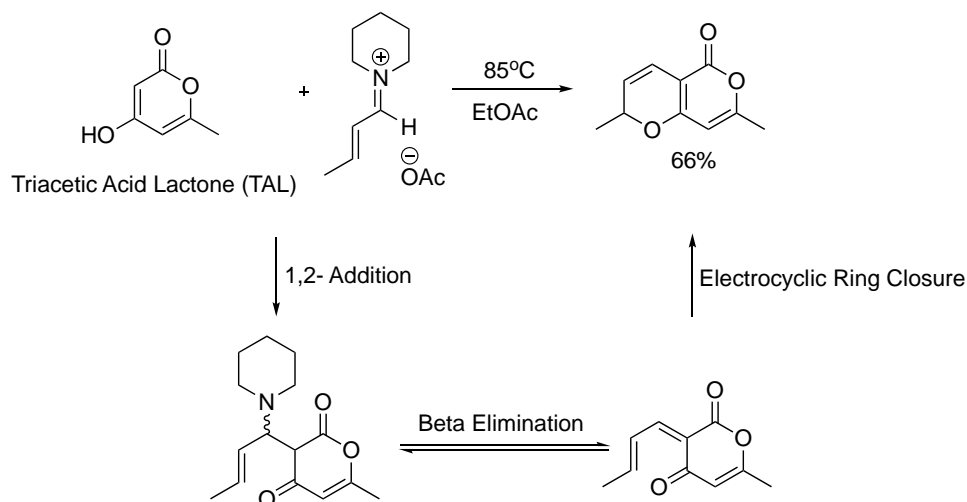


Figure 2.2. Sequential 1,2-addition for [3+3] cycloadditions

The condensation of this system requires a dual electrophile, which is capable of undergoing a 1,2-addition as well as a 1,4-addition. If an aldehyde is used in place of an iminium ion, high regioselectivity is lost, and several side products form.⁷ For the Knoevenagel (Figure 2.3) condensation aldehydes lack regioselectivity in comparison to the iminium ion which can undergo beta-elimination allowing a 6π electron system.

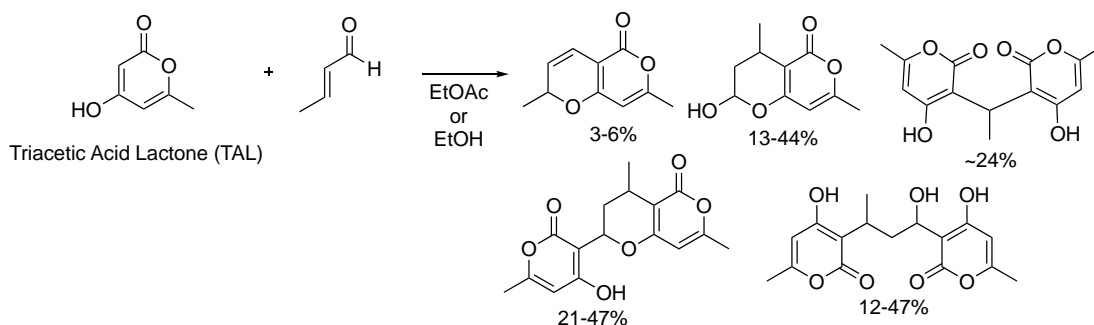


Figure 2.3. Side reactions for Knoevenagel [3+3] condensation.

Another example of a [3+3] reaction used in the literature is the total synthesis Hippodamine.⁸ In this total synthesis the [3+3] cycloaddition uses an iminium ion as a catalyst. (Figure 2.4) In this reaction a 1,2-addition occurs with the iminium ion and the alpha carbon of the ester, followed by the 6π ring closure. To complete the synthesis of Hippodamine the tricyclic ester underwent hydrogenation, epimerization and decarboxylation to remove the ester group.⁹

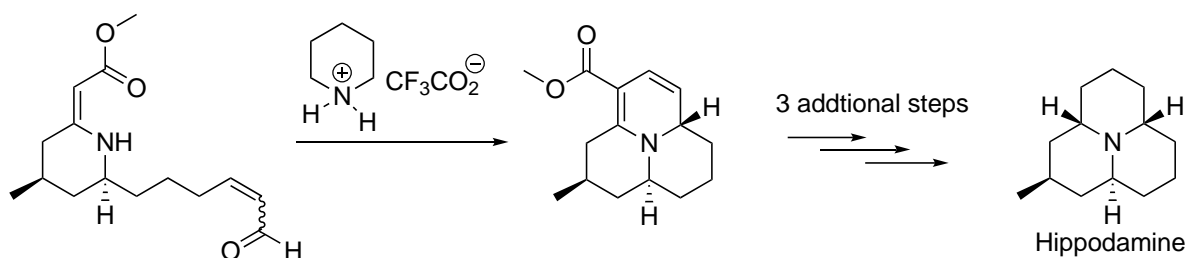


Figure 2.4. Synthesis of Hippodamine, highlighting the [3+3] cycloaddition

Lastly, an example of the total synthesis is of Pyripyropene-A using a oxa [3+3] reaction, which is utilized with an unsaturated acid chloride (Figure 2.5).¹⁰ Hsung showed that the 4-hydroxypyronone is acylated by the acid chloride. After the acylation a 1,3-acyl migration occurs followed by a 1,4 addition. The [3+3] reaction of the unsaturated acid chloride with the 3-hydroxypyronone gives a dihydro-4H-pyran-4-one moiety. After the reduction with NaBH_4 , the synthesis of Pyripyropene A was complete.

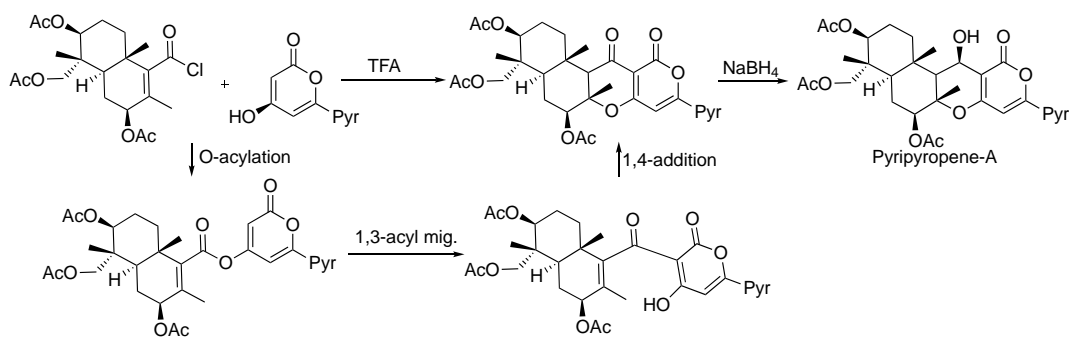


Figure 2.5. Total synthesis of Pyripyropene-A

Instead of using an aldehyde or iminium ion, an acyl group can be used. In the [3+3] reactions with unsaturated acid chlorides, there are two distinct possibilities (Figure 2.6).¹¹ TAL could react with crotonic acid in acidic conditions to allow the 1,3 acyl migration to occur. In basic conditions there is no migration, instead a conjugate addition occurs.

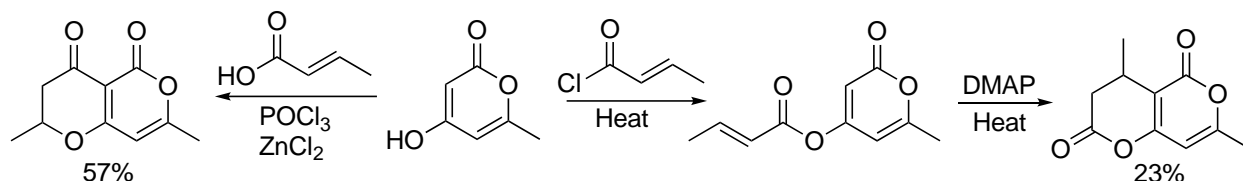


Figure 2.6. Regioselectivity of [3+3] with unsaturated acid chloride

The chromone moiety is present in a variety of bioactive compounds. Representative compounds include the chromones shown in Figure 2.7. Several researchers have reported pathways to γ -pyrones and chromones. Although the literature on γ -pyrone synthesis is more extensive, a number of flexible routes to γ -pyrones and chromones have been described. Much of the work on γ -pyrones was collected in timely reviews by Moses,¹² Lee,¹³ and Borges.¹⁴ Chromone **1** was isolated from the marine mangrove fungus ZZF41 from the South China Sea. It exhibited cytotoxicity towards KB and KBv200.¹⁵ Amides of chromone **2** are potent nontoxic inhibitors specific for the breast cancer resistance protein.¹⁶ Bromochromone **3** is a key intermediate in the Silva synthesis of xanthenes.¹⁷ Chromone **4** was isolated from *A. barbadensis*, a succulent that has been used in traditional medicine.¹⁸ Compound **5** was reported as part of a study of bioactive neoflavones.¹⁹

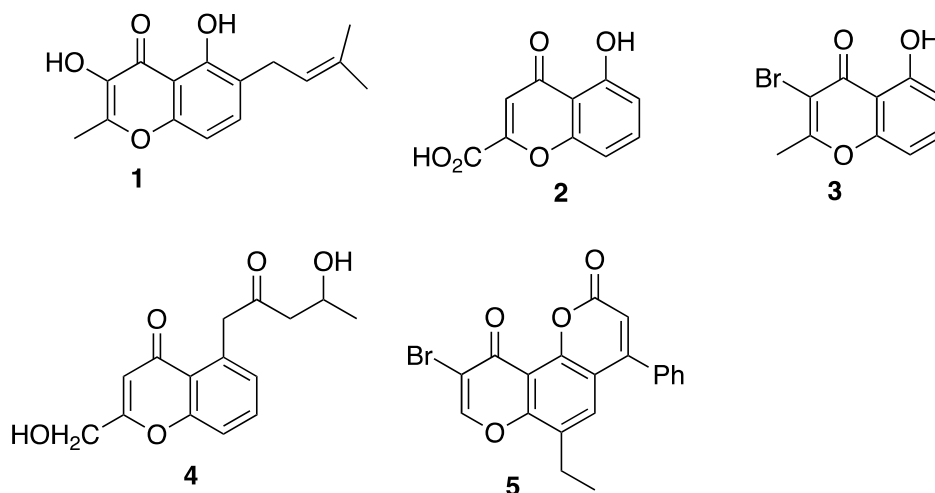
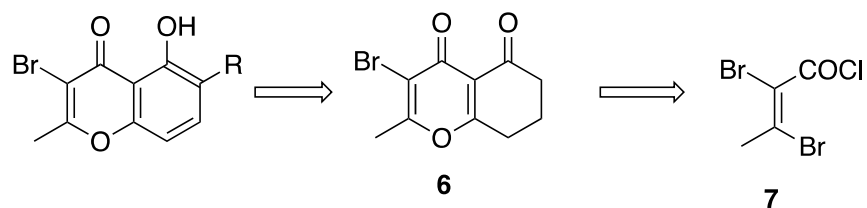


Figure 2.7. Structures of chromones.

2.2. Results

The retrosynthetic pathway is illustrated below in Scheme 2.1. The connection of a haloacryloyl chloride with a keto ester has precedent in the work of Gelin.^{20,21} The 2,3-dichloroacryloyl chloride was synthesized by the method of Haurert.²² Dibromobutenoyl chloride **7** was synthesized by bromination of 2-butynoic acid. The halopyrone **6** was viewed as an intermediate for elaboration into chromones **1**, **2**, **3** or **4**.

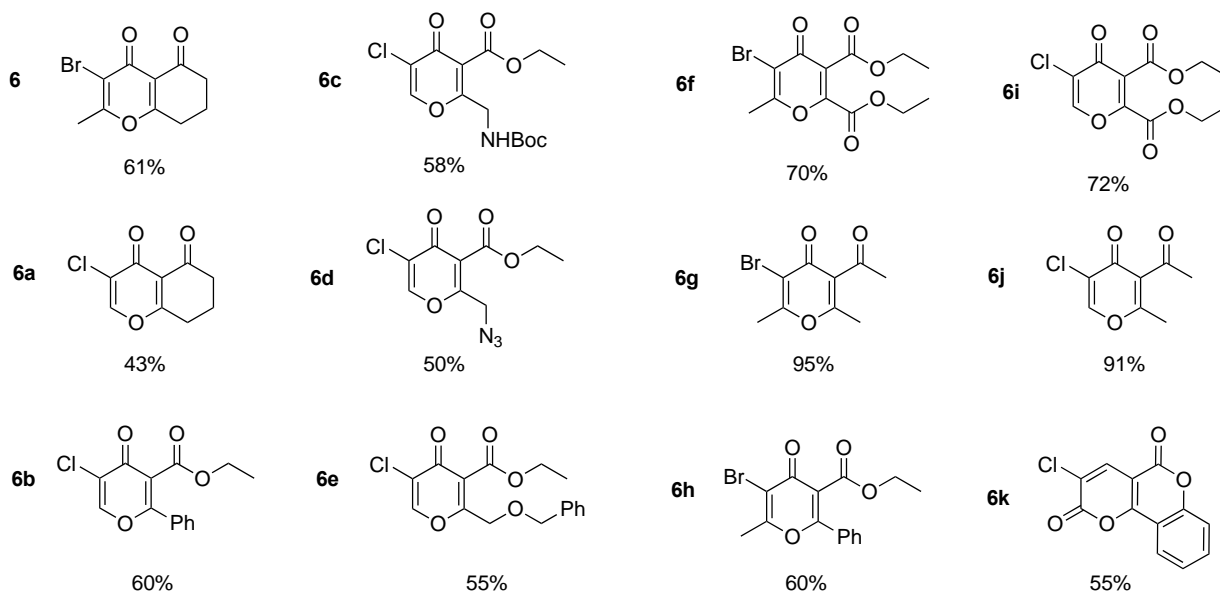


Scheme 2.1. Retrosynthetic approach

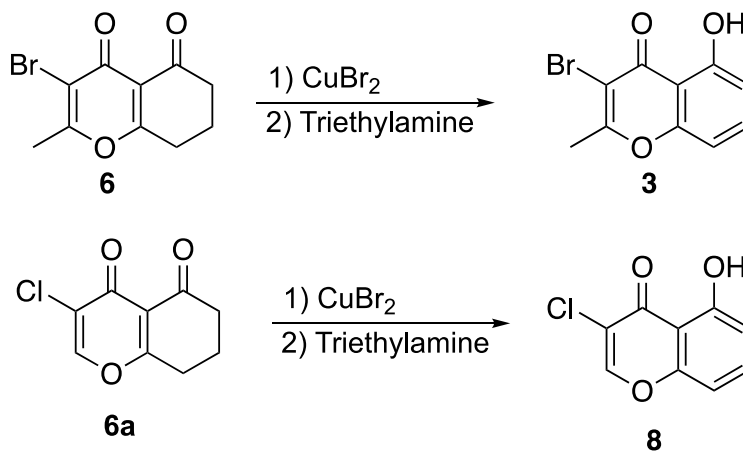
Table 1 shows the scope of this reaction. Both cyclic and acyclic dicarbonyl compounds participate in the reaction. Cyclic products **6** and **6a** reacted at 135 °C in THF rather than 60 °C for **6c-6j** to close the γ -pyrones ring. Higher temperatures were required possibly due to strain of forming the bicyclic product. Azides and carbamates are tolerated in the reaction.

Interestingly, 4-hydroxycoumarin formed product **6k** in 55% yield, demonstrating that the 4-hydroxycoumarin was unable to undergo a 1,3 acyl migration.

Table 2.1. Scope of [3+3] for γ -pyrones

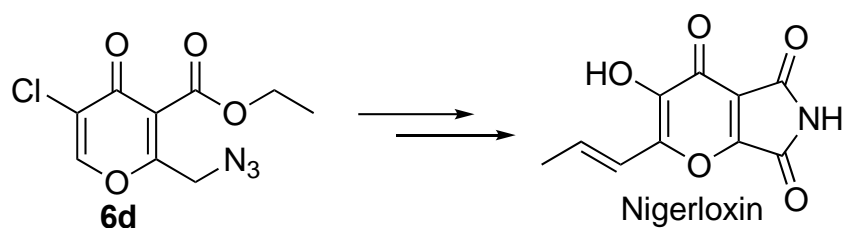


The aromatization of **6** to **3** was studied. Initially, aromatization using DDQ was explored. However, no chromone-containing product was observed. Fortunately, bromination with copper bromide of **6** followed by treatment with base provided chromones **3** and **8** in 95% and 85% overall yield, respectively.



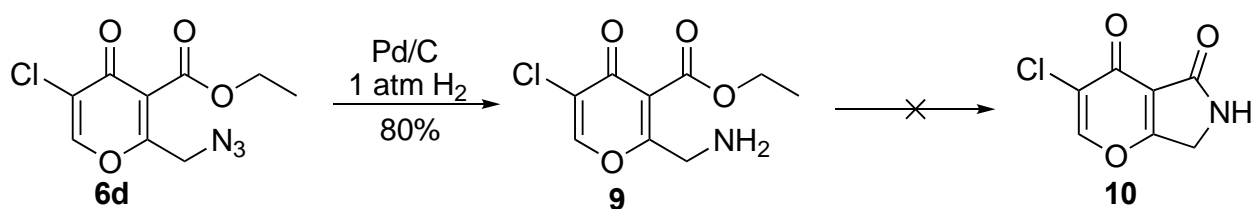
Scheme 2.2. Aromatization of **6** and **6a**

The γ -pyrone **6d** was unable to be converted into the natural product nigerloxin (Scheme 2.3). This natural product, fermented from *Aspergillus niger*, is a rat lens aldose reductase inhibitor as well as a radical scavenger.²³ The bioactivity made nigerloxin an interesting target for synthesis.



Scheme 2.3. Proposed synthesis of Nigerloxin

However, attempts to convert **6d** to Nigerloxin failed due to the unsuccessful conversion from **9** to **10**. Product **6d** was converted to **9** by hydrogenation of azide with Pd/C. Attempts to convert **9** to **10** consisted of the following conditions: NaH in THF, BF₃ etherate in CH₂Cl₂, TiCl₄ in CH₂Cl₂, and heating reaction up to 130°C. The synthesis of **10** was unsuccessful due to ring strain of the γ -pyrone.



Scheme 2.4. Attempts to synthesize **10**

While synthesis of nigerloxin was unsuccessful, it was found that **6d** showed bioactivity. Each product in the **6-6k** series were tested for antimicrobial activity. Molecule **6d** contains an azide moiety, a functional group that has numerous pharmaceutical applications.²⁴ In this series **6d** showed a promising level of antimicrobial activity in comparison to cetylpyridinium chloride, (CPC) a commercially used antimicrobial agent. Each experiment measured the zone of

inhibition of a substrate. A larger the zone of inhibition (ZOI) referred to a greater effect in antimicrobial activity. CPC was found to inhibit *E. coli* ATCC 25922 with a ZOI of 11.31 mm and inhibited *S. Typhimurium* ATCC 14028 with a ZOI of 11.1 mm. In Tables 2.2 and 2.3, molecule **6d** showed was competitive with CPC, in both *E. Coli* ATCC 25922 and *S. Typhimurium* ATCC 14028 strains. When **6d** had chelator agent ethylenediaminetetraacetic acid (EDTA) introduced, the combination of the two increased the overall ZOI by 3.77 mm in *E. coli* ATCC 25922 and 1.29 mm in *S. Typhimurium* ATCC 14028. The increase of ZOI after the introduction of EDTA as a chelator agent to the **6d** substrate mixture led us to test the ZOI of **11** (Figure 2.8).

Table 2.2. Antimicrobial effect of inhibitors for *E. coli* ATCC 25922

No inhibitor	CPC	6d	6d + 50 mM EDTA	11
0 mm	11.31 mm	13.04 mm	16.81 mm	12.63 mm

Table 2.3. Antimicrobial effect of inhibitors for *S. Typhimurium* ATCC 14028

No Inhibitor	CPC	6d	6d + 25mM EDTA	11
0 mm	11.1 mm	10.15 mm	12.39 mm	12.42 mm

Molecule **11** not only contains a γ -pyrone and azide moiety, but also contains an enolic alpha-diketone. This moiety is an effective chelator agent for various metals. The synthesis of **11** was based on the Ashooriha synthesis.²⁵ Interestingly, **11** has no reported antimicrobial activity. Substrate **11** was found to be an effective antimicrobial agent at 12.63 mm ZOI for *E. coli* ATCC 25922 and 12.42 mm ZOI for *S. Typhimurium* ATCC 14028, indicating there was

little difference in antimicrobial activity between **6d** and **11**. In future studies, the γ -pyrone azide moiety will need to be studied for toxicity for humans and stability due to the reactive nature of organic azides.

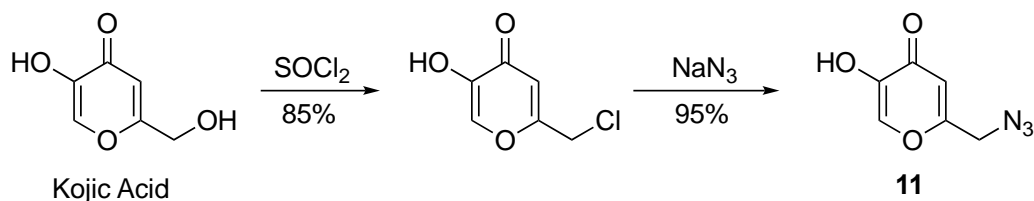


Figure 2.8. The synthesis of 11

2.3. Conclusion

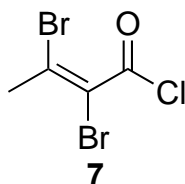
In this chapter, we have developed a direct synthesis of functionalized γ -pyrones and 5-hydroxychromones. In the synthesis of γ -pyrones, we synthesized 12 different halo γ -pyrones. Bicyclic γ -pyrones were then converted into 5-hydroxychromones in moderate yields. Attempted synthesis of nigerloxin was unsuccessful due to the inability to close the lactam ring. However, **6d** was found to be a potentially valuable antimicrobial agent. Future studies will be conducted to further show the applications of **6d**.

2.4. Experimental

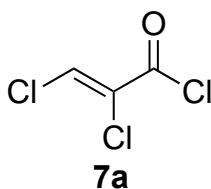
2.4.1. General information

All starting materials were purchased from Sigma-Aldrich, AK Scientific Institution and Oakwood Chemical; Solvents were all purchased from Sigma-Aldrich and Fisher Scientific, and used without further distillation. All reactions were monitored by thin layer chromatography (TLC) and ^1H NMR. All yields refer to separated yield after column chromatography unless indicated. TLC was obtained by silica plate using UV light as a visualizing agent or Potassium permanganate solution with heat. All columns were performed with silica gel 60Å, particle size

40-63 μm . ^1H and ^{13}C NMR spectra were acquired in CDCl_3 or other deuterated solvents on a Varian MR-400 or Bruker Avance III 600 MHz spectrometer.



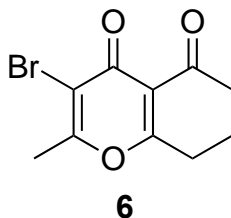
2,3-Dibromo-2-butenoyl chloride (7). The 10 g of 2,3-dibromo-2-butenic acid was then added to excess oxalyl chloride dissolved in 30 mL of 1,2-dichloroethane. After addition of the carboxylic acid, a single drop of dimethylformamide was added to the solution and the exit gas was passed through a bubbler with sodium hydroxide bath. After the addition of all materials to the solution, the reaction was heated to $70\text{ }^\circ\text{C}$ for 3 hours. Excess oxalyl chloride and 1,2-dichloroethane was removed by reduced pressure at $40\text{ }^\circ\text{C}$ yielding a dark oil. ^1H NMR (400 MHz, Chloroform-d) δ 2.54 (s, 1H). ^{13}C NMR (101 MHz, Chloroform-d) δ 167.45, 135.66, 107.06, 29.35.



2,3-dichloroacryloyl chloride (7a). Added solid 20 g of mucochloric acid to a 60mL of 5M solution of NaOH over the course of 20 minutes at $0\text{ }^\circ\text{C}$. The solution was then slowly heated to $50\text{ }^\circ\text{C}$. The solution would turn to an orange color. After 2 hours the reaction was cooled to $0\text{ }^\circ\text{C}$ and 20mL of 12M HCl was added dropwise. A precipitate was formed and was then filtered and

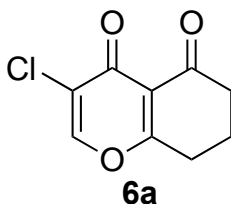
washed with cold H₂O. ¹H NMR (400 MHz, Chloroform-d) δ 11.29 (s, 1H), 7.81 (s, 1H). ¹³C NMR (101 MHz, DMSO-d₆) δ 161.81, 131.72, 128.94. MS 139.94 M/Z.

The carboxylic acid was then added to 2 eq of oxalyl chloride dissolved in 1,2-dichloroethane. After addition of the carboxylic acid, a single drop of dimethylformamide was added to the solution and was attached to a bubbler with 1 M sodium hydroxide bath. After the addition of all materials to the solution, the reaction was heated to 70 °C for 3 hours. Excess oxalyl chloride and 1,2-dichloroethane was removed by lowered pressure at 40 °C yielding a dark oil. Hexanes was then added to the oil resulting in a dark precipitate, which was then removed by filtration. Followed by further solvent removal by lowering pressure and evaporation at 40 °C collecting a clear oil at 56% yield. ¹H NMR (400 MHz, Chloroform-d) δ 8.10 (s, 1H). ¹³C NMR (101 MHz, Chloroform-d) δ 160.43, 140.13, 131.24.

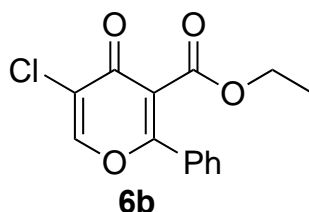


3-bromo-2-methyl-7,8-dihydro-4H-chromene-4,5(6H)-dione (6). Molecule **6** was prepared from mixing 1 mmol of 1,3-cyclohexanedione with 2 mmol of sodium hydride in 5 mL of THF in a 25 mL sealable tube. Then molecule **7**, which was dissolved in 2 mL of THF, was added dropwise to the solution. The mixture was sparged with argon, the reaction was sealed, and was heated slowly to 135 °C for 6 hours. After the reaction was cooled to room temperature, then 10 mL of 1M HCl was added to the mixture. The mixture was then extracted with 3 x 30 mL of ethyl acetate, dried with sodium sulfate, and solvent was removed in vacuo to a dark oil. The oil was then separated with column chromatography with 4:1 solution of hexanes: ethyl acetate. Molecule **6** was isolated in 61% yield. ¹H NMR (400 MHz, CDCl₃) δ 2.87 (t, J = 6.3 Hz, 2H),

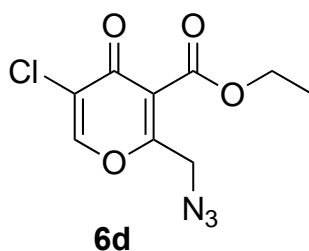
2.68 (s, 3H), 2.58 (dd, $J = 7.4, 6.0$ Hz, 2H), 2.16-2.08 (m, 2H). ^{13}C NMR (100MHz CDCl_3) δ 194.76, 172.08, 156.19, 154.18, 115.00, 111.69, 38.58, 28.85, 22.33, 19.49. MS 253 M/Z



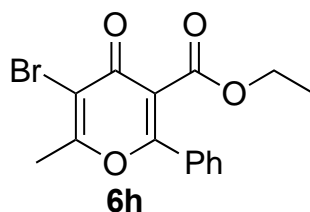
6a ^1H NMR (400 MHz, CDCl_3) δ 7.97 (s, 1H), 2.88 (t, $J = 6.5$ Hz, 2H), 2.57 (t, $J = 6.7$, 2H) 2.24-2.14 (m, 2H). ^{13}C NMR (101MHz CDCl_3) δ 192.87, 172.17, 157.00, 136.42, 120.93, 114.65, 36.25, 27.73, 20.18. MS 200 M/Z. **6a** was isolated in 43% yield.



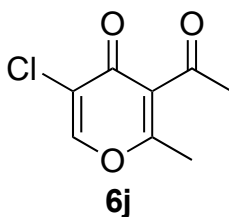
6b ^1H NMR (400 MHz, CDCl_3) δ 8.21 (s 1H), 7.66 (m, H2), 7.55 (d, $J = 9.6$ Hz, 1H), 7.52 (m, 2H), 4.26 (q, $J = 7.2$ Hz, 2H), 1.17 (t, $J = 7.2$ Hz, 3H). ^{13}C NMR (100MHz) δ 170.16, 163.65, 163.08, 151.74, 131.93, 130.35, 128.90, 127.37, 109.99, 77.24. 62.32, 13.78 MS 278. **6b** was isolated in 60% yield.



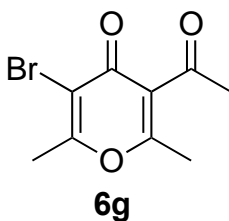
6d 50% yield. ^1H NMR (400 MHz, Chloroform- d) δ 8.05 (s, 1H), 4.40 (q, $J = 7.1$ Hz, 2H), 4.33 (s, 2H), 1.37 (t, $J = 7.1$ Hz, 3H). ^{13}C NMR (100 MHz, Chloroform- d) δ 169.09, 162.60, 162.54, 151.46, 126.65, 122.00, 62.74, 49.67, 14.05. MS 257 M/Z. **6d** was isolated in 50% yield



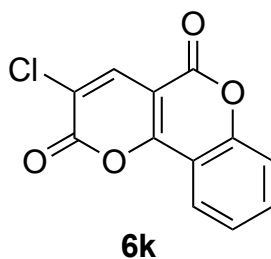
6e 55% yield. ¹H NMR (400 MHz, CDCl₃) δ 7.67-7.58 (m, H₂), 7.59-7.49 (m, 1H), 7.52-7.42 (m, 2H), 4.26 (q, J = 7.2 Hz, 2H), 2.61 (s, 3H), 1.17 (t, J = 7.2 Hz, 3H). ¹³C NMR (100MHz) δ 170.43, 163.96, 163.55, 161.81, 131.61, 130.58, 128.85, 127.77, 114.21, 62.16, 13.81 MS 336 M/Z. **6h** was isolated in 60% yield



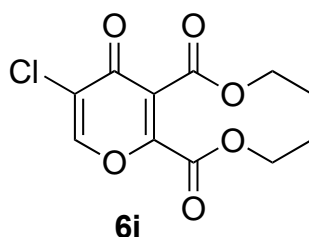
6j 50% yield. ¹H NMR (400 MHz, CDCl₃) δ 7.96 (s H=1), 2.56 (s H=3), 2.38 (s H=3) ¹³C NMR (101MHz) δ 199.16, 177.10, 168.01, 151.25, 126.60, 126.31, 31.96, 18.84 MS 186 M/Z. **6j** was isolated in 91% yield



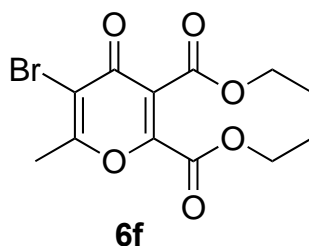
¹H NMR (400 MHz, Chloroform-d) δ 2.56 (s, 3H), 2.51 (s, 3H), 2.37 (s, 3H). ¹³C NMR (101MHz) δ 195.16, 177.10, 168.01, 151.25, 126.60, 126.31, 31.96, 20.11, 18.84. MS 243 M/Z. **6g** was isolated in 95% yield.



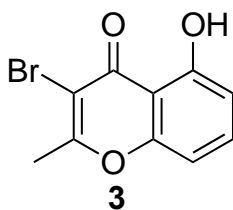
¹H NMR (600 MHz, Chloroform-d) δ 8.17 (s, 1H), 8.10 (d, $J = 7.9$ Hz, 1H), 7.75 (t, $J = 7.9$ Hz, 1H), 7.47 (q, $J = 8.7, 8.0$ Hz, 2H). ¹³C NMR (151 MHz, Chloroform-d) δ 160.05, 157.93, 155.40, 153.39, 137.57, 134.87, 125.56, 123.53, 122.10, 117.56, 112.65, 103.57. MS 247 M/Z. **6k** was isolated in 55% yield.



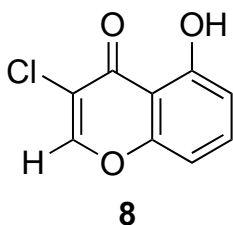
¹H NMR (400 MHz, Chloroform-d) δ 8.09 (s, 1H), 4.41 (qd, $J = 7.1, 0.9$ Hz, 4H), 1.37 (td, $J = 7.2, 4.7$ Hz, 6H). ¹³C NMR (101 MHz, Chloroform-d) δ 169.99, 161.73, 158.35, 151.77, 149.53, 133.78, 127.25, 126.12, 63.82, 62.77, 13.89. MS 274 M/Z. **6i** was isolated in 72% yield.



¹H NMR (400 MHz, Chloroform-d) δ 4.41 (qd, $J = 7.2, 1.6$ Hz, 4H), 2.62 (s, 3H), 1.37 (td, $J = 7.1, 4.6$ Hz, 6H). MS 331 M/Z. **6f** was isolated in 70% yield.



Synthesis of 3. To a mixture of 1mmol of **6** in 5mL of ethyl acetate, 2 mmol of CuBr₂ was added. The reaction was heated for 12 hours at 80°C. The reaction mixture was cooled to room temperature and was filtered. The solvent was removed in vacuo, then the crude product was dissolved in 4 mL of dimethyl formamide. Subsequently, 4 mmol of triethylamine was added dropwise over 10 minutes. The reaction was stirred at room temperature for 12 hours. Afterwards, 20 mL of 1M HCl was added to the mixture. The mixture was then extracted 4 times with 10 mL of CH₂Cl₂, washed 2 times with 50 mL of 1M HCl and washed with brine. The oil was then separated by column chromatography with 5:1 solution of hexanes: ethyl acetate. The product was isolated in 95% yield. ¹H NMR (400 MHz, DMSO) δ 10.91 (s, 1H), 7.40 (t, J = 8.2 Hz, 1H), 6.81 (d, J = 8.2 Hz, 2H), 2.79 (s, 3H). ¹³C NMR (101MHz, DMSO) δ 206.45, 156.71, 156.44, 153.24, 153.24, 153.16, 132.76, 112.31, 111.27, 110.40, 109.14, 107.53, 24.46 MS 253 M/Z



¹H NMR (400 MHz, Acetonitrile-d₃) δ 8.26 (s, 1H), 8.14 (s, 1H), 7.43 (td, J = 8.3, 1.0 Hz, 1H), 6.92 – 6.80 (m, 2H). ¹³C NMR (101MHz, Acetonitrile-d₃) δ 206.45, 156.71, 156.44, 153.24, 153.24, 153.16, 132.76, 112.31, 111.27, 110.40, 109.14, 107.53. MS 195 M/Z. **8** was isolated in 85% yield.

2.4.2. Agar overlay

Start with overnight growth of desired microbe for testing at 37°C overnight. Developed a 1:10 dilution (1 part culture into 10 parts PBS) of overnight culture in phosphate buffered saline. This will give us 10^8 CFU/mL in this suspension. Made overlay agar, this has a lower concentration of agar (0.75%). Then began adding agar to this concentration to regular TSB. Autoclave this and temper it (cool it) to 50 °C if not tempered, it will be too hot and will kill the bacteria when we add them to it later. Poured agar plates regular concentration of agar (1.5%). These will serve as a solid support and their inherent color will provide some contrast to make zones of inhibition more clearly visible. Take culture suspensions –add 0.5 mL of these to sterile 15 mL polypropylene tubes. Add 4.5 mL of tempered 0.75% overlay agar, mix thoroughly via vortex. This creates an agar overlay containing cells to be tested containing 10^7 CFU/mL. Pour the seeded overlay (seeded with our test cells) onto the base agar plates and let solidify. When this grows up, we will get a solid lawn cells. In a clean, sterile petri dish, you will saturate a blank sterile paper disk (6mm diameter) with our test compounds by adding only as much as can be absorbed by the disk –any additional compound will cause inconsistent results. For essential oils, this is typically around 25 mL of oil, but this may vary according to what compound you are testing. Using clean/sterile forceps, aseptically add disk to seeded agar overlay, let attach for a few minutes and invert and incubate overnight at 37°C. If the agent being tested is antimicrobial, it will diffuse radially outward and inhibit growth of the lawn, as evidenced by a zone of clearing or inhibition, also known as ZOI (zone of inhibition). All ZOI values were measured from the bottom of the plate with a digital caliper. Each compound was tested in triplicate, with a negative control of DMSO only on the filter.

2.5. References

- [1] Sheldon, R. A. *Green Chem.* **2014**, 16, 950–963.
- [2] Kwak, M. Y.; Rhee, J. S.; “Cultivation characteristics of immobilized *Aspergillus oryzae* for kojic acid production,” *Biotechnology and Bioengineering* **1992**, 39, 9, pp. 903–906.
- [3] Watanabe, K.; Iwasaki, K.; Abe, T.; Inoue, M.; Suzuki, T.; Katoh, T. *Org. Lett.* **2005**, 7, 17, 3745-3748
- [4] Wulff, H.; Beeton, C.; Chandy, K. G. *Curr. Opin. Drug DiscoVery DeV.* **2003**, 6, 640.
- [5] Hsung, R. P.; Shen, H. C.; Douglas, C. J.; Morgan, C. D.; Degen, S. J.; Yao, L. J. *J. Org. Chem.* **1999**, 64, 690-691.
- [6] Kametani, T.; Kajiwara, M.; Fukumoto, K. *Tetrahedron* **1974**, 30, 1053-1058.
- [7] de March, P.; Moreno-Manas, M.; Casado, J.; Pleixats, R.; Roca, J. L.; Trius, A. J. *Hetrocycl. Chem.* **1984**, 21, 1369-1370.
- [8] Gerayuto, A. I.; Hsung, R. P. *Org. Lett.* **2006**, 8, 4899-4902.
- [9] Gerayuto, A. I.; Hsung, R. P. *Org. Lett.* **2007**, 72, 2476-2484.
- [10] Shen, H. C.; Degen, S. J.; Mulder, J. A. Hsung, R. P.; Douglas, C. J.; Golding, G. M.; Johnson, E. W.; Mathias, D. S.; Morgan, C. D.; Mueller, K. L.; Shih, R. A. In 216th ACS National Meeting, Boston, MA, Fall, **1998**, Abstract No. ORGN-664.
- [11] Zehnder, L. R.; Dahl, J. W.; Hsung, R. P. *Tetrahedron Lett.* **2000**, 41, 1901-1905.
- [12] Sharma, P.; Powell, K. J.; Burnley, J.; Awaad, A. S.; Moses, J. E. *Synthesis* **2011**, 2865-92.
- [13] Lee, J. S. *Marine Drugs* **2015**, 13(3), 1581-1620.
- [14] Gaspar, A.; Matos, M. J.; Garrido, J.; Uriarte, E.; Borges, F. *Chem. Reviews* **2014**, 114, 4960-4992.
- [15] Huang, Z.; She, Z.; Cai, X.; Lin, Y.; Zhou, S. *Zhongshan Daxue Xuebao, Ziran Kexue ban* **2009**, 48(6), 63-68.
- [16] Valdameri, Glaucio; Genoux-Bastide, Estelle; Peres, Basile; Gauthier, Charlotte; Guitton, Jerome; Terreux, Raphael; Winnischofer, Sheila M. B.; Rocha, Maria E. M.; Boumendjel, Ahcene; Di Pietro, Attilio, *Journal of Medicinal Chemistry* **2012**, 55(2), 966-970.

- [17] Santos, C. M. M.; Silva, Artur M. S.; Cavaleiro, J. A. S. *European J. Org. Chem.* **2009**, 2642-2660.
- [18] Wu, X.; Yin, S.; Zhong, J.; Ding, W.; Wan, J.; Xie, Z. *Fitoterapia* **2012**, 83, 1706.
- [19] Moskvina, V. S.; Khilya, V. P.; Turov, O. V.; Groth, U. M. *Synthesis* **2009**, 1279.
- [20] Chanteorel, B.; Nadi, A. I.; Gelin, S. *Synthesis* **1982**, 1107.
- [21] Gelin, S.; Gelin, R. *Bull. Soc. Chem. Fr.* **1969**, 231.
- [22] Haunert, Frank and Goetz, Norbert PCT Int. Appl., 2007019210, 15 Feb 2007 (IS 18)
Prepared from reaction of oxalyl chloride with the acid (Org. Synth. 2008, 85, 231).
- [23] Rao, K. C.; Divakar, S.; Babu, K. N.; Rao, A. G.; Karanth, N. G.; Suttur, A. P. *Journal of Antibiotics* **2002**, 55(9): 789-793.
- [24] Tanimoto, H.; Kakiuchi, K.; *Natural Product Communications* **2013**, 8(7), 1021-1034.
- [25] Ashooriha, M.; Khoshneviszadeh, M.; Moradi, R. A.; Kardan, M.; Emami, S. *Bioorganic Chemistry* **2019**, 82, 414-422.

CHAPTER 3. APPLICATIONS OF CITRIC AND MALIC ACID

William Bradley, Yang Qu, George Kraus

3.1. Introduction

3.1.1. Citric acid and malic acid

Citric acid and malic acid are tri- and diacids developed from bio-renewable sources. Citric acid is a fermentation product from various different fungi. The first fermentation was completed by 1893 by the strain *Penicillium glaucum*.¹ In 2007, 1.6 million tons of citric acid were produced worldwide. Citric acid is a triacid with a tertiary alcohol (Figure 3.1).

In 2016, malic acid and citric acid had market sizes of 159 million dollars and 2.5 billion dollars, respectively.² Reactions that transform these feedstock acids into more valuable materials are needed. There are many fruits that have high concentration of citric and malic acid. These fruits include cranberries, apricots, and grapefruit.

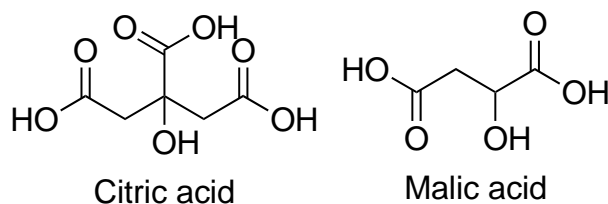
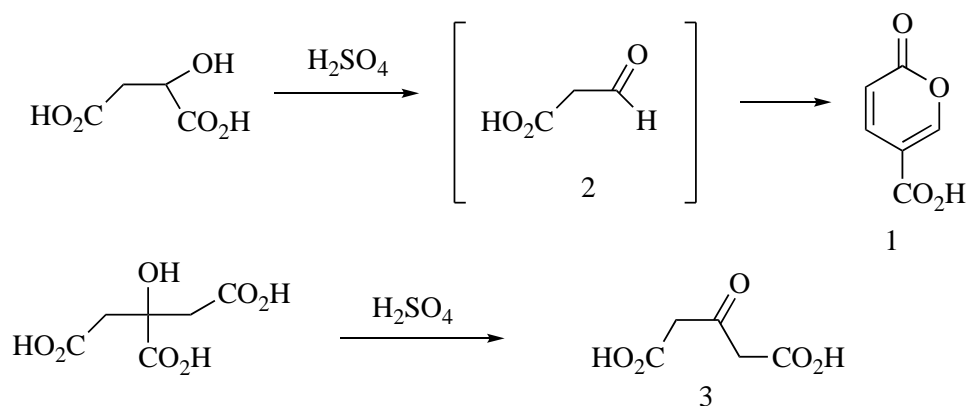


Figure 3.1. Structure of citric acid and malic acid

3.1.2. Von Pechmann reaction

The reaction of hydroxy acids with strong acids such as sulfuric acid has a long history. In 1893 von Pechmann reported that the reaction of malic acid in hot sulfuric acid produced coumalic acid **1**, as shown in Scheme 3.1.³ In this reaction, an aldehyde acid **2** was generated along with carbon monoxide. The aldehyde acid was not stable under the reaction conditions and dimerized to coumalic acid (Scheme 3.1). Citric acid, when treated with sulfuric acid at 80

°C, produces acetone dicarboxylic acid **3** in 90% yield. (Scheme 3.1).⁴ Other hydroxy acids such as tartaric acid,⁵ mandelic acids,⁶ and quinic acid⁷ also undergo this reaction.



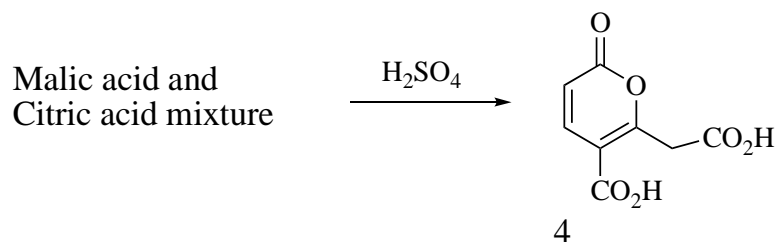
Scheme 3.1. Conversion of malic acid to coumalic acid from decarbonylation intermediate

There are many fruits that have high concentration of citric and malic acid. Separating both acids from one another is difficult, due to multiple carboxylic acids functional groups. Here we propose transformations that can use both acids together to develop novel products.

3.2. Results

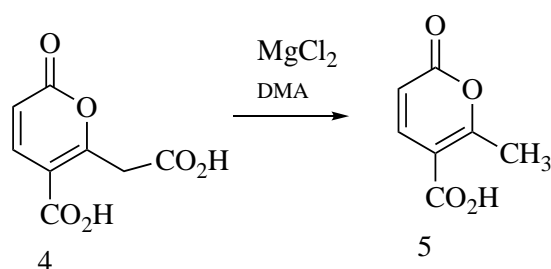
3.2.1 Diacid pyrone synthesis

As part of a project to understand the chemistry of mixed organic acids and esters, we reacted a 1:1 mixture of citric acid and malic acid in concentrated sulfuric acid at 80 °C. To our surprise, the product was not a mixture of **1** and **3** but a new material in 45% yield whose structure we determined to be pyrone **4** (Scheme 3.2).



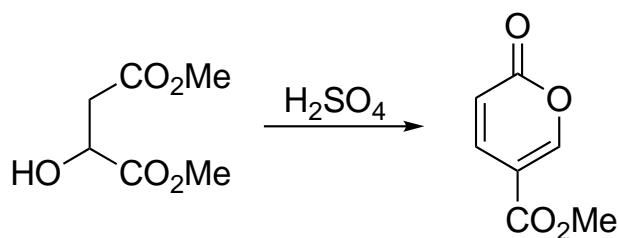
Scheme 3.2. Synthesis of 4 with mixture of Malic acid and Citric acid

Diacid **4** was formed by the reaction of the aldehyde acid from malic acid with acetone dicarboxylic acid produced from citric acid. The yield of diacid **4** could be increased to 76% by adding 2 equivalents of citric acid. Diacid **4** is a new pyrone and has functionality useful for making sustainable polymers. A related pyrone, 4,6- pyrone dicarboxylic acid, is produced from lignin via biocatalysis and has been converted into polymers.⁸ With catalytic magnesium chloride in boiling dimethylacetamide (DMA) diacid **4** was regioselectivity decarboxylated to acid **5** in 95% yield as shown in Scheme 3.3.⁸



Scheme 3.3. Selective decarboxylation of 4

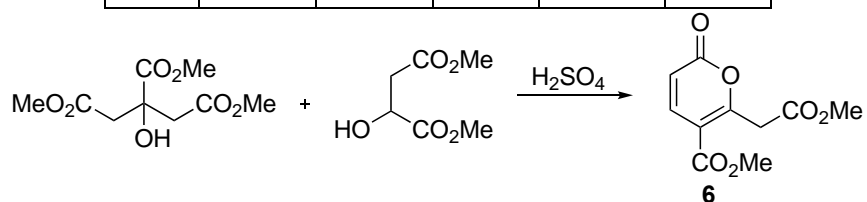
Although the production of coumalic acid is well preceded, we have not found any precedent for converting a *hydroxy ester* into an aldehyde. This pathway might have a number of advantages over the route from malic acid. If the reaction was successful, the resulting coumalate ester would be much less water soluble than coumalic acid. Esters such as dimethyl malate or diethyl malate are commercially available. As shown in Scheme 3.4, the reaction of dimethyl malate with sulfuric acid in 1,2-dichlorethane affords methyl coumalate in 84% isolated yield as a white solid. Its proton NMR spectrum matched the literature spectrum. This reaction could be scaled to produce 10 grams of methyl coumalate. Different malate-sulfuric acid ratios were tested: four equivalents of sulfuric acid per equivalent of malate gave the best result. The reaction did not proceed below 80 °C.



Scheme 3.4. Synthesis of methyl coumalate

Table 3.1. Reaction table of scheme 3.4. Reactions occurred over 12 hours.

Entry	Diester (mmol)	H ₂ SO ₄ (mmol)	Temp. (°C)	Co- solvent (10 mL)	yield
1	4.5	9	80	Neat	43%
2	4.5	13.5	80	Neat	67%
3	4.5	18	80	Neat	82%
4	4.5	22.5	80	Neat	81%
5	4.5	18	80	DCE	84%
6	4.5	18	80	CH ₃ CN	messy
7	4.5	18	80	1,4- Dioxane	NR
8	4.5	18	80	CH ₃ NO ₂	messy
9	4.5	18	60	DCE	NR
10	4.5	18	100	DCE	84%



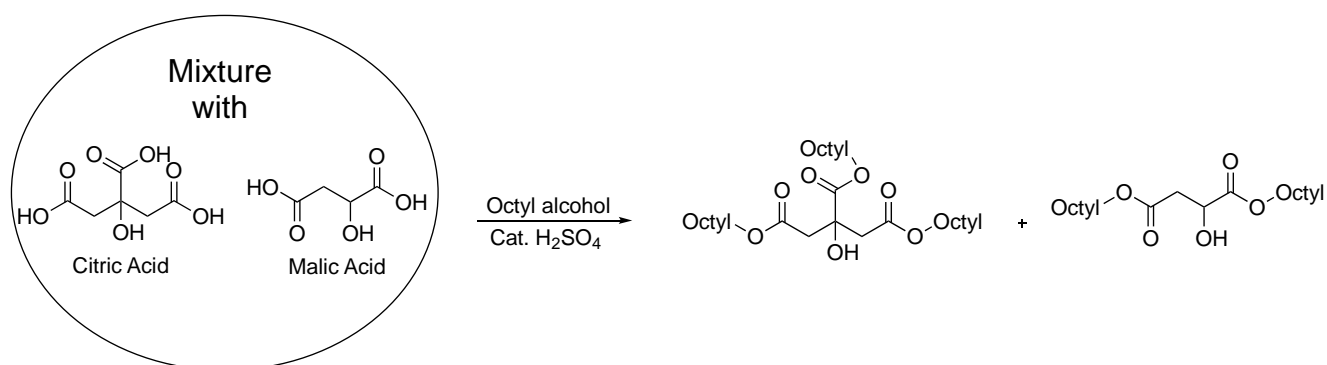
Scheme 3.5. Synthesis of **6** methyl citrate and methyl malate

The mixture of dimethyl malate and trimethyl citrate afforded diester **5** in 50% yield as shown in Scheme 3.5. Use of a 1.3:1 ratio of citrate to malate afforded **5** in 55% yield. In Table

1 different solvents were used with varying amounts of sulfuric acid. In these reactions it was found that 4 equivalents of sulfuric acid were necessary to convert the methyl malate to methyl coumalate. The use of dichloroethane resulted in a clear product, in comparison to the other solvents used.

3.2.2. Plasticizer mixture synthesis

In the case where citric acid and malic acid are in solutions with various sugars from a plant source. With the application of Fischer esterification, a simple extraction with ethyl acetate was able to separate out the citric and malic octyl ester. Octyl alcohol was used to add hydrophobic chains to the carboxylic acids yet can be removed with distillation.



Scheme 3.6. Synthesis of plasticizer solution

Citric and malic octyl esters were unable to be separated. These octyl esters were then utilized as a mixture to be a plasticizer for poly lactic acid (PLA) at a MW = 100,000 g/mol. Dioctyl phthalate, a known plasticizer, was used to compare the plasticizer mixture composed of citrate and malate esters. Differential Scanning Calorimetry (DSC) was used to measure the blend of PLA with the plasticizers. The plasticizer mixture of octyl citrate/malate esters were found to be competitive with the dioctyl phthalate ester with a 1.7% and 4.3% differential between the two for the 5% and 20% blend of plasticizers respectively. The mixture octyl citrate and malate esters can be used with PLA to allow for a bio-based polymer system. The lowered

T_g of PLA increased the elasticity aspect of the polymer system. In the future it would be possible to use longer and branched alcohols. Octyl alcohol was ideal for this experiment due to the ease of distillation, compared to larger alcohols.

Table 3.2. PLA Glass Transition change from addition of plasticizer

Plasticizer Blend	Glass Transition
PLA (MW 100,000 g/mol)	62.3°C
PLA/5% Dioctyl Phthalate	52.7°C
PLA/5% Dioctyl Citrate/Malate Esters	54.4°C
PLA/20% Dioctyl Phthalate	34.4°C
PLA/20% Dioctyl Citrate/Malate Esters	38.7°C

3.3. Conclusion

The reaction of mixed acids or esters provides a rapid route to a novel pyrone. These pyrones can be produced on gram scales from biorenewable sources. The procedure using diesters⁹ offers an improved yield and is an operationally more convenient route to synthesize methyl coumalate. This chapter also implemented the mixture of acids to be converted into an effective plasticizer mixture. Importantly, the esters are preserved and allow for a direct synthesis of pyrones **4** and **6**. Overall, this chapter can be characterized by the ability to convert complex inexpensive mixtures to higher value materials.

3.4. Experimental

3.4.1. General information

All starting materials were purchased from Sigma-Aldrich, AK Scientific Institution and Oakwood Chemical; Solvents were all purchased from Sigma-Aldrich and Fisher Scientific, and

used without further distillation. All reactions were monitored by thin layer chromatography (TLC) and ^1H NMR. All yields refer to separated yield after column chromatography unless indicated. TLC was obtained by silica plate using UV light as a visualizing agent or Potassium permanganate solution with heat. All columns were performed with silica gel 60\AA , particle size 40-63 μm . ^1H and ^{13}C NMR spectra were acquired in CDCl_3 or other deuterated solvents on a Varian MR-400 or Bruker Avance III 600 MHz spectrometer.

Procedure for making methyl coumalate from dimethyl malate: To a flame dried round bottom flask was added dimethyl malate (729 mg, 4.5 mmol) followed by concentrated sulfuric acid (1 mL, 18 mmol) and dichloroethane (3 mL). The reaction mixture was heated to $80\text{ }^\circ\text{C}$ for 12 hours. After cooling to room temperature, the brown reaction mixture was poured onto 40 g ice and stirred for 30 min. The mixture was extracted with ethyl acetate ($3 \times 20\text{ mL}$) and the combined organic extracts were washed with ice-cold water and dried over anhydrous sodium sulfate. Concentration and flash chromatography gave methyl coumalate in 84% yield. ^1H NMR (400 MHz, CDCl_3) δ 8.3 (dd, $J = 2.6, 1.1\text{ Hz}$, 1H), 7.8 (dd, $J = 9.8, 2.6\text{ Hz}$, 1H), 6.3 (dd, $J = 9.8, 1.1\text{ Hz}$, 1H), 3.9 (s, 2H).

Procedure for 4: To a flame dried round bottom flask was added malic acid (1 g, 7.46 mmol) and citric acid (2.86 g, 14.9 mmol) followed by the addition of concentrated sulfuric acid (2 mL, 36 mmol). The reaction was heated to $80\text{ }^\circ\text{C}$ for 12 hours. After cooling to room temperature, the brown reaction mixture was poured to 40 g of ice and stirred for 30 min. The mixture was extracted with ethyl acetate ($3 \times 20\text{ mL}$). The combined organic extracts were washed with ice-cold water, dried over anhydrous sodium sulfate, concentrated and collected in 76% yield. ^1H NMR (400MHz, DMSO) δ 7.86 (d, $J = 9.8\text{ Hz}$, 1H), δ 6.33(d, $J = 9.8\text{ Hz}$, 1H), δ 3.98 (s, 2H).

Procedure for 5: To a flame dried round bottom flask was added malic acid (1 g, 6.17 mmol) and trimethyl citrate (2.86 g, 12.2 mmol) followed by the addition of concentrated sulfuric acid (2 mL, 36 mmol), and 5 mL of dichloroethane. The reaction was heated to 80 °C for 12 hours. After cooling to room temperature, the brown reaction mixture was poured onto 100 g of ice and stirred for 30 min. The mixture was extracted with ethyl acetate (3 × 20mL) and the combined organic extracts were washed with ice-cold water and dried over anhydrous sodium sulfate. Concentration and flash chromatography gave **5** 55% yield ¹H NMR (400 MHz, CDCl₃) δ 7.84 (d, *J* = 9.8 Hz, 1H), δ 6.28 (d, *J* = 9.8 Hz, 1H), δ 4.07 (s, 2H), δ 3.85 (s, 3H), δ 3.74 (s, 3H).

Development of plasticizer mixture: To a flame dried round bottom flask was added mixture of citric and malic acid was added followed by excess of octyl alcohol as solvent. The reaction was heated to 80°C and a single drop of H₂SO₄ was added. The reaction was allowed to stir for 12 hours. After cooling to room temperature, the yellow reaction mixture was extracted with ethyl acetate (3 × 20mL) and the combined organic extracts were washed with ice-cold water and dried over anhydrous sodium sulfate. The reaction was then heated to 130°C under 40mTorr to remove any contaminants of octyl alcohol. The mixture of plasticizers were then magnetically stirred in a 20 mL vial with PLA at 100°C/oven at the desired concentration.

3.4.2. Differential scanning calorimetry (DSC)

The DSC measurement was taken from TA DSC Q2000 differential scanning calorimeter operating under nitrogen atmosphere. Samples underwent two cycles of heating and cooling process at 20°C/min and 10°C/min, respectively. The glass transition temperatures (T_gs) were taken from the second heating cycle.

3.5. References

- [1] Grand View Research, Citric Acid Market Size, *Share & Trends Analysis Report By End Use* **2018**, GVR
- [2] Grand View Research, Malic Acid Market Size, *Share & Trends Analysis Report By* **2019**, GVR-2-68038-083-5
- [3] von Pechmann, *Ann.* 1891, 264, 272. Wiley, R. H.; Smith, N. R., *Organic Syntheses* **1963**, Vol. 4, 201.
- [4] Wu, H.; Li, Y.; Liu, Y.; Lyu, S.; Wu, C.; Li, T. *ChemBioChem* **2012**, 13(6), 862-871.
- [5] Hilbert, G. E. *J. Am. Chem. Soc.* **1932**, 54, 3413.
- [6] Harada, K.; Aoi, M.; Shirai, M. *Jpn. Kokai Tokkyo Koho* **1995**, JP 07258246 A 19951009.
- [7] Assoah, B.; Veiros, L. F.; Afonso, C. A. M.; Candeias, N. R. *Eur. J. Org Chem.* **2016**, 3856–3861.
- [8] Qian, Y.; Otsuka, Y.; Sonoki, T; Mukhopadhyay, B.; Nakamura, M.; Jellison, J.; Goodell, B. *BioResources* **2016**, 11(3), 6097-6109.

CHAPTER 4. BLENDING THE EFFECTIVENESS OF ANIONIC POLYMERIZATION WITH THE VERSITILITY OF RAFT BY USE OF THE ATOM TRANSFER RADICAL ADDITION-FRAGMENTATION TECHNIQUE

Michael Forrester, William Bradley, Fang-Yi Lin, Nacu Hernandez, Chris Williams, George Kraus, and Eric Cochran. Michael Forrester and William Bradley are coauthors

4.1 Introduction

Anionic polymerization has been used industrially since the mid 20th century to produce many well-defined polymers with a variety of chain architectures.¹ For example, poly(styrene-*b*-butadiene-*b*-styrene) (SBS) has been used extensively as a modifier for asphalt.² Polybutadiene is commonly used to manufacture tire treads and carcasses.³ Anionic polymerization consistently produces well-defined polymers with dispersity (\bar{D}) frequently less than 1.1, and is readily applied to diverse array of monomer types including vinyl aromatics, dienes, certain ring opening monomers, and others. It efficiently achieves conversions exceeding 99% in fewer than four hours. Despite these advantages, anionic polymerization has its limitations. For instance, the carbanion active center will readily react with most electrophilic groups at rates competitive with monomer propagation. Significantly, many vinyl and (meth)acrylic compounds will not yield high molecular weight polymers without sub-freezing reaction temperatures,⁴ a prohibitively costly prerequisite for most commercial applications.

4.1.1 Controlled radical polymerization

The dawn of reversible deactivation radical polymerization (RDRP, also commonly referred to as controlled radical polymerization) in the 1990s has opened some interesting doors for producing an array of new block copolymers. In general, these methods drastically limit the free radical concentration, driving the rate of termination reactions to nearly negligible levels.

For example, atom transfer radical polymerization (ATRP) is one of the most commonly

researched RDRP techniques.⁵ ATRP is suitable for a wide variety of monomers including vinyl aromatics, (meth)acrylics, and vinylics. A well-designed ATRP will achieve good molecular weight control with dispersity values $1.1 < \mathcal{D} < 1.5$. Some drawbacks include sluggish reaction kinetics with vinyl aromatics and an inability to control diene polymerization.⁶ Another undesirable aspect is the requirement of a homogeneous transition metal catalyst, commonly copper, that presents challenges with respect to separations, toxicity and environmental stewardship.⁷ ATRP is also particularly sensitive to oxidants and other contaminants.⁷ Progress continues in addressing these issues, for example with adaptations such as the ARGET⁸ (Activators ReGenerated by Electron Transfer) and ICAR⁹ (Initiators for Continuous Activator Regeneration) implementations. Nonetheless, with these adaptations number average molecular weights (M_n) greater than $M_n > 100$ kDa and $\mathcal{D} < 1.5$ are difficult targets, requiring prohibitively long reaction times.¹⁰ Additionally, the ARGET/ICAR methods place restrictions on solvent selection, often forcing the use of expensive and nonvolatile candidates such as dimethylformamide or anisole.⁸ Thus, the reduction of transition metal use comes at the price of extended long reaction times, additional separations challenges and costly solvents. Widespread commercial adoption will require that these challenges be addressed. The Reversible Addition Fragmentation Chain Transfer (RAFT) polymerization method was published three years after ATRP.¹¹ It has since proven to be a reliable polymerization technique for producing block copolymers of controlled molecular weight and low dispersity. Like ATRP, RAFT is compatible with a large library of vinyl monomers. However, RAFT also suffers from sluggish kinetics with vinyl aromatic monomers. While RAFT can be used to control diene polymerization, temperatures greater than 120°C are required to achieve reasonable kinetics; under these conditions thermally tolerant chain transfer agents must be used and crosslinking is

problematic.¹² Unlike ATRP, RAFT does not require the use of transition metals, rather relying on a chain transfer agent (CTA) that reversibly associates with chain ends to control the molecular weight. The CTA typically comprises a thiocarbonyl compound such as a dithioester, trithiocarbonate, xanthate, or dithiocarbamate.¹¹ The activity and controllability of a CTA toward different functional monomers relies on functional groups that accompany the thiocarbonyl center. While the R group leaves as a free radical when activated, the Z group modifies the kinetics of RAFT process by stabilizing the intermediate radical-deactivated CTA structure. RAFT, in contrast to ATRP and anionic polymerization, has the advantage of being more compatible with functional groups, less sensitive to impurities, and more tolerant of solvent choice.⁹

4.1.2 Block-copolymer

The advantages of the RAFT and anionic polymerization techniques are complementary: anionic polymerization efficiently produces vinyl aromatics and dienes, while RAFT polymerization offers access to a host of other vinyl-based monomers. For this reason, techniques for the sequential application of both methods would enable the construction of a much broader palette of heterogeneous copolymers. Styrene/diene based block copolymers, which are used extensively in various industries such as paving and construction,¹³ adhesives,¹⁴ and paints and coatings,¹⁵ could be supplanted with styrene/butyl acrylate analogs. A natural strategy for the marriage of RAFT and anionic polymerization is the construction of CTA functionality from the terminus of a living polyanion. Zhang et al. achieved this by adding carbon disulfide to a diphenylethylenecapped polyisoprene.¹⁶ While this method was up to 95% efficient and offered a flexible selection of R groups, a number of drawbacks limit its reduction to commercial practice. Most notably, cryogenic temperatures are required to produce the macro-CTA. Additionally, the Z-group is restricted to the diphenylethylene end group of the terminated

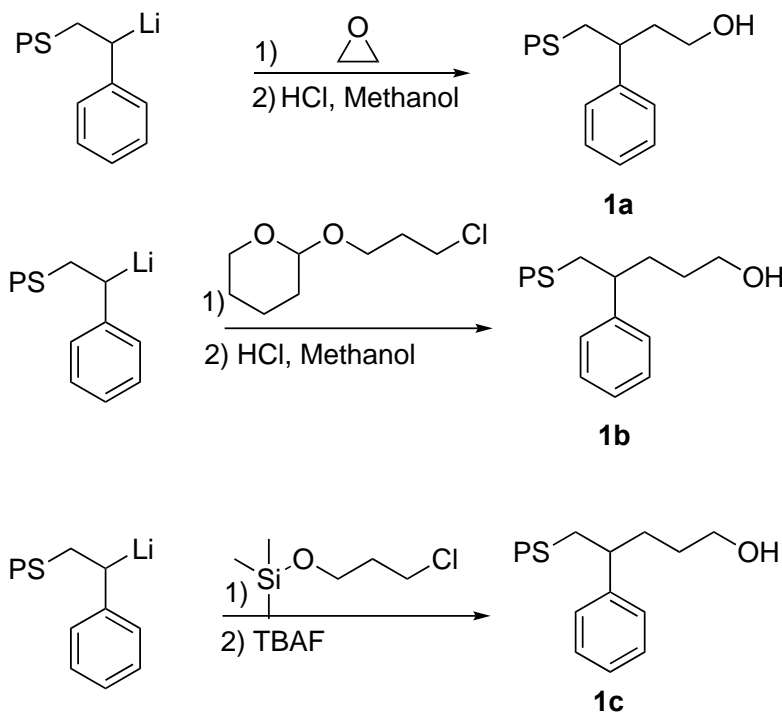
carbanion; accordingly, other desirable Z groups such as xanthate, phenyl dithioester, trithiocarbamate, and dithiocarbamate are inaccessible through this method. Furthermore, the anionic- and RAFT-based blocks are joined through the thioester linkage, potentially limiting the thermal and chemical stability of the final product.¹⁷ Yin et al. reported a macroCTA produced through the esterification of a hydroxy-terminated polymer with an acidfunctionalized CTA.¹⁸ While yields were not reported, our own experiments using this approach were roughly 50% efficient. Nonetheless, these examples illustrate the utility of transforming anionically produced polymers into macro-CTAs. In this work we illustrate the use of the atom-transfer radical addition-fragmentation (ATRAF) reaction that was developed by the Matyjaszewski group¹⁹ as a highly efficient and potentially scalable route to hybrid anionic/RAFT block copolymers.

4.2 Results

4.2.1 Polystyrene end-group modification

Various implementations of this process are shown in Schemes 1 and 2. Short reaction times, high conversion and yield, and mild reaction temperatures make this an appealing approach to macro-CTA fabrication. In addition to exemplifying the application of ATRAF to the marriage of anionic and RAFT polymerizations, we also investigate the practicality of reduced-copper/copper-free adaptations that would result in a more economical and scalable process. Additionally, we explore alternatives to ethylene oxide in building the intermediate ester linkage in this process, namely through acetal or silane functionalized capping agents. A list of materials that were made are summarized in Table 1.; experimental details are provided in the Supporting Information. Table 1. shows the results from the various steps of making macro-CTA from living anionic polymerization. Homopolymer molecular weights were determined by polystyrene calibrated gel permeation chromatography (GPC); block copolymer molecular weights are estimated using that of the homopolymer precursor and composition measured by

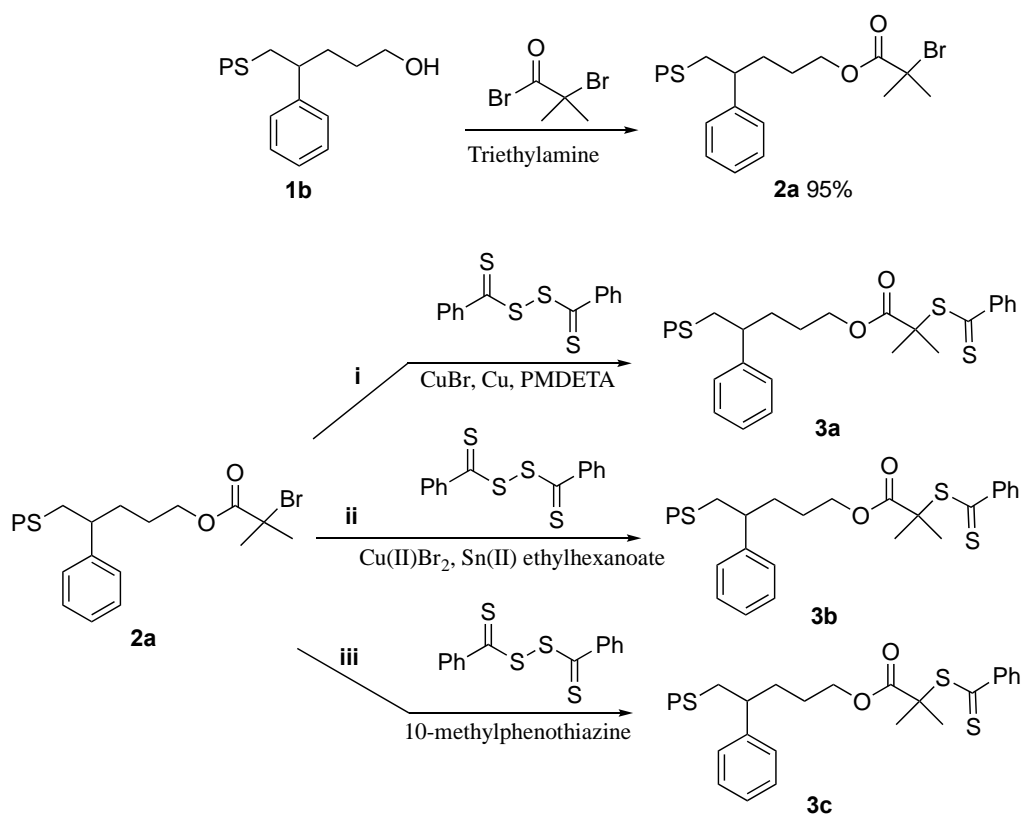
NMR. Efficiencies are determined by either NMR or GPC and are denoted in the table. Further details are available in experimental section. In the first step, hydroxyl functionality is added to the living carbanion. In Scheme 4.1, this is achieved through the addition of ethylene oxide followed by acidic methanol 1a.



Scheme 4.1. Chemical scheme for various routes to hydroxyl terminated polystyrene: (a) Ethylene oxide termination with acidic workup ($R = -(CH_2)_2-$); (b) termination with 2-(3-chloropropoxy)-tetrahydro-2Hpyran followed by hydrolysis of the acetal ($R = -(CH_2)_3-$); and (c) (3-chloropropoxy)trimethylsilane termination followed by cleavage with TBAF ($R = -(CH_2)_3-$).

Alternatively, hydroxyl functionality can be provided quantitatively with significantly less toxic reagents. For example, the carbanion can be quenched by a halogenated acetal that can be further hydrolyzed (1b). Halogenated silane-protected alcohol can also be used and subsequently cleaved with tetrabutylammonium fluoride (TBAF) to provide the alcohol (1c). GPC (Figure 1a) suggests chain-end modification through a subtle shift in the elution volume

between PS-H and the corresponding PS-OH. ¹H-NMR end group analysis (Figures 4.9) definitively shows approximately 1 alcohol per chain, irrespective of the route chosen with near 100% molar conversion. Yields were nearly quantitative with slight losses (< 3%) due to handling during workup. Hydroxyl terminated polystyrene was converted to tertbromine capped polystyrene with a stoichiometric excess of 2-bromo-2-methylpropanoyl bromide (2a), which proceeds to completion as supported by NMR (Figure 4.8) and GPC (Figure 4.1 (a)). Bis(thiobenzoyl)disulfide (TBDS) provides the final macro-chain transfer agent functionality through the ATRAF method. Direct characterization of macro-CTA functionality proved to be difficult. Proton resonances in ¹H-NMR from the thioate chain

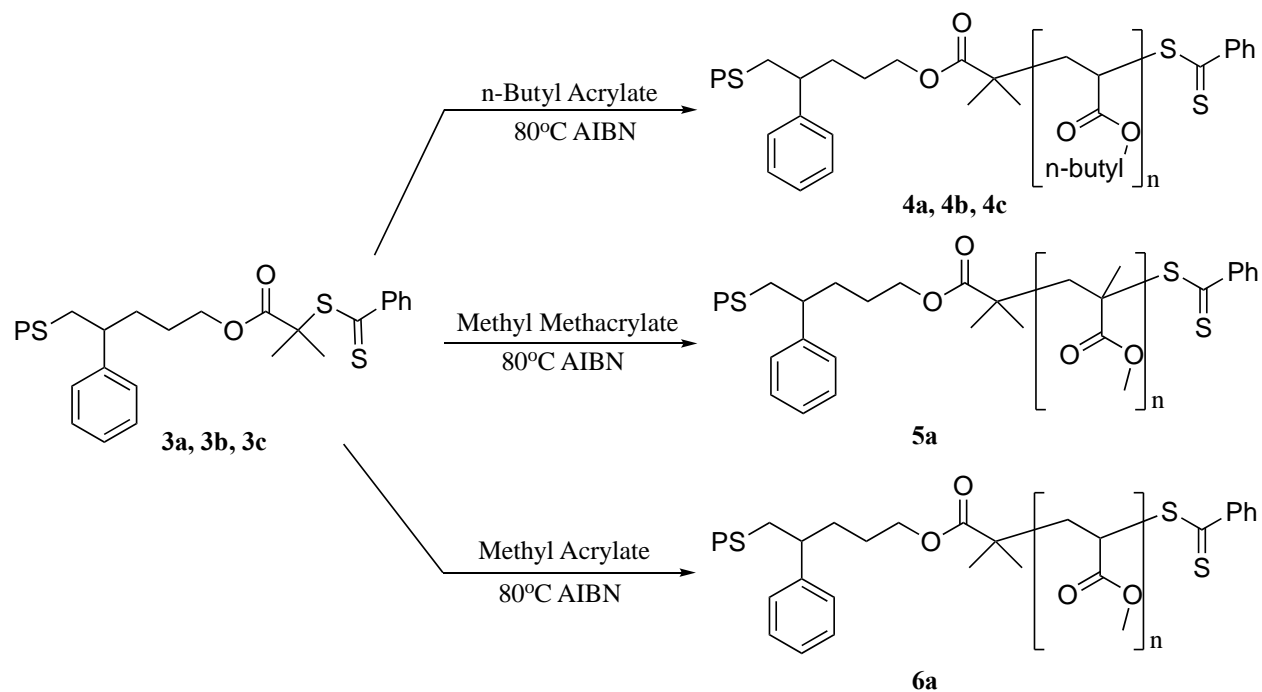


Scheme 4.2. Chemical scheme for the halogenation (2a–2c) of PS-OH followed by construction of a macroCTA using ATRAF via the (i) traditional, (ii) ARGET-mediated, and (iii) Photoredox catalyzed metal-free methods.

ends overlap with those of the polymer, which compounded by their low prevalence as a chain-end moiety are undetectable; ^{13}C -NMR experiments were also unable to discern the relevant carbon atoms. While GPC chromatograms show slight shifts in elution volume upon each chain-end modification, this provides only a weak qualitative indication of CTA attachment and no guarantee of activity. Accordingly, the most efficacious manner in which to quantify the macro-CTA activity is to produce a di-block copolymer.

4.2.2. Di-block copolymer development

To judge the activity with multiple classes of radically polymerizable species, styrenic block copolymers were synthesized with *n*-butyl acrylate (4a-4c), methyl methacrylate (5a) and methyl acrylate (6a) as demonstrated in Scheme 4.3.



*Scheme 4.3. Chemical scheme of RAFT block co-polymers synthesized from anionic polymerization produced macro chain transfer agent with (1) *n*-butyl acrylate, (2) methyl methacrylate and (3) methyl acrylate.*

The detection of the new polymeric species formed at 254 nm with UV detection is a strong indication that block copolymer was formed, as only the polystyrene block is detectable in this manner, as shown in Figure 4.1 (b). The ratio of the integrated value of the polystyrene homopolymer peak to the block copolymer peak yields the fraction of active macro-CTA. We recorded efficiencies as high as a 97% in this manner as shown in Table 4.1 for polymerization with methyl acrylate, n-butyl acrylate, and methyl methacrylate. These block copolymers under phase separation as expected; for example, differential scanning calorimetry, rheology and transmission electron microscopy data are provided in the Supporting Information and show a microphase separated lamellar morphology. The “traditional” ATRAF (3a) method is evidently 97% efficient in producing active macro-CTA. Here we note that while phenyl is a robust choice for the Z-group, the use of TBDS is exemplary in nature and could easily be substituted for other disulfides as appropriate for other Z-groups. The ARGET methodology can be used to drastically reduce the requisite quantity of transition metal catalyst. This was illustrated using sub-stoichiometric quantities of copper (II) bromide and tin (II) ethylhexanoate (SnEtH) as the

Table 4.1. Results of polymerization of PS-macro-CTA with various different monomer sources

- a- Molar conversions of chain end to -OH or -Br per ¹H-NMR
- b- H-NMR CTA resonances overlap with polymer
- c- Polystyrene-CTA precursor
- d- Overall Molecular weight computed from precursor molecular weight and ¹HNMR block copolymer composition.
- e- Corresponding to the deblock copolymer peak extracted from the GPC chromatogram via peak deconvolution
- f- Fraction of RAFT-active chains per GPC peak deconvolution

Polymer Code	M _n , kDa	PDI	Efficiency
1a	10	1.11	100% ^a

Table 4.1. (continued).

1b	10.5	1.06	100% ^a
1c	9.4	1.15	100% ^a
2a	11.8	1.15	100% ^a
3a	12.3	1.17	— ^b
3b	11.5	1.25	— ^b
3c	13	1.1	— ^b
4a	10, ^c 67	1.37 ^e	97% ^f
4b	10, ^c 200	4 ^e	30% ^f
4c	10, ^c 30%	2.6 ^e	30% ^f
5a	10, ^c 55.5 ^d	1.37 ^e	82% ^f
6a	10, ^c 37 ^d	1.31 ^e	93% ^f

reducing agent. We noted that TBDS was susceptible to attack by the reducing agent, and were able to successfully afford **3b** by alternating SnEtH and TBDS addition. While the efficiency of the macro-CTA was reduced to 30%, these experiments demonstrate ARGET ATRAF is a viable approach that could be improved with further optimization of reaction conditions and the selection of reducing agent. The most ideal approach would be to completely remove the use of transition metal catalysts. To achieve this, we utilized a method very similar to that described by Treat et al. 20 in which a phenothiazine species activated by ultraviolet radiation was used as a photocatalyst to perform ATRP. While the Treat et al. team achieved the best balance of activation/deactivation rates using 10-phenylphenothiazine, we found that the readily available 10-methylphenothiazine was

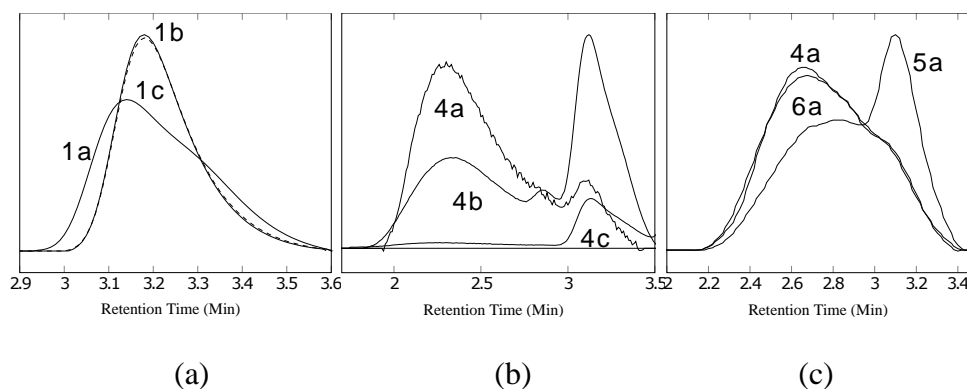


Figure 4.1. The GPC chromatogram (a) shows the small shift from polystyrene aliquot (**1b**), to ethylene oxide capped (**1a**), to tert-butyl bromide capped (**2a**). The chromatogram (b) shows the growth of *n*-butyl acrylate using traditional ATRAF (**4a**), ARGET (**4b**), and metal-free method (**4c**). The chromatogram (c) shows the growth of *n*-butyl acrylate (**4a**), methyl methacrylate (**5a**), and methyl acrylate (**6a**)

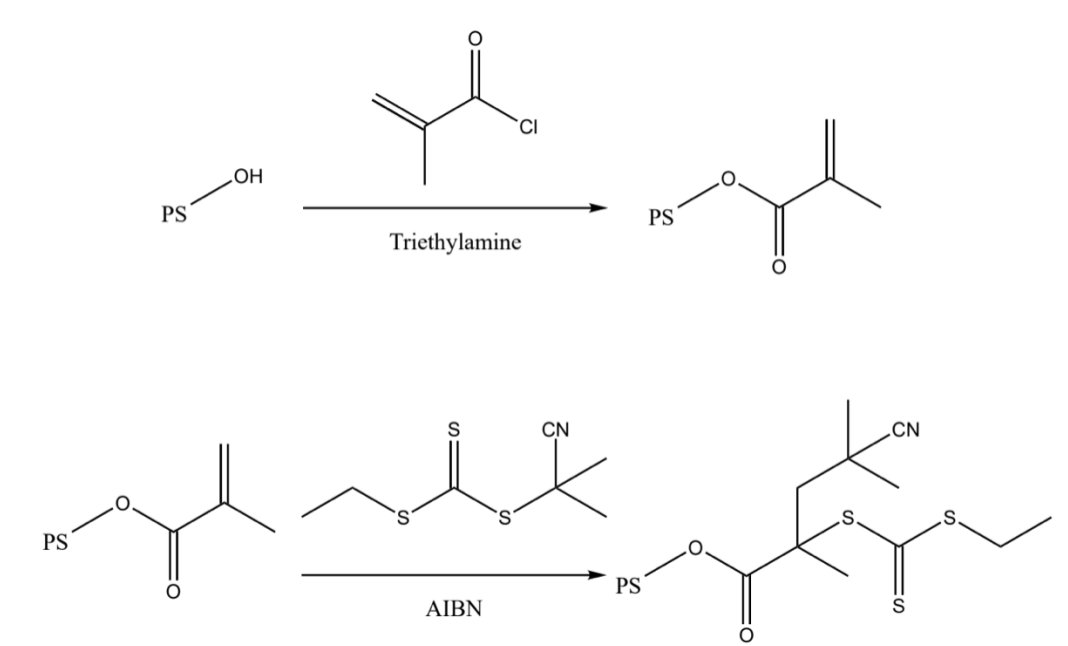
adequate since only a single activation/deactivation event is necessary. While the resultant macro-CTA produced block copolymer, the molecular weight distribution was quite broad and only 30% of the parent polystyrene was converted to diblock. We believe that a large factor of the lower conversion is that the particular wavelength of the UV radiation we used may damage the CTA species and further optimization of reaction conditions could render this method as an attractive candidate for producing metal-free RAFT CTA's.

4.2.3 Macromonomers

Macromonomers can also be utilized to produce macro-CTAs. This method was designed to have no impurities requiring purification past steam coagulation. The utilization of a small molecule chain transfer agent (CTA) with a macromonomer to be converted to a macro CTA was first performed by Houshyar.²¹ In our work, we are able to insert a single macromonomer-polystyrene onto a CTA to form a macro-CTA. The macromonomer methodology from polystyrene had advantages over the ATRAF method discussed above due to the lack of metals

and fewer other impurities. The macromonomer method allowed for the maintaining of quick reaction times and high conversion rates of block copolymer efficiency.

Different monomers will influence which CTA is used and will affect the choice of additional blocks. In this work, only meth acrylics were tested (Scheme 4.4), but acrylics and vinyls should be possible. For example, polymethacrylate is used for the second block, a methacrylate macromonomer will be developed. In the case where polyacrylic or polyvinyl are desired for the second block then a macromonomer with the corresponding monomer attached. Once these various macromonomers and various CTAs have been studied this will allow for a very versatile route for producing anionic-RAFT copolymers.



Scheme 4.4. Schematic for single insertion of macromonomer to produce macro-CTA

Molecular weight of the polymer was determined by GPC and HNMR to confirm that quantitative amounts of alcohol functionality existed on the polymer end-group. In Figure 4.2 it can be seen the alkene source of 1 macromonomer per chain end group on the polymer. The reaction of a CTA and with the styrene macromonomer resulted in the development of a macro-

CTA. This reaction was heated at 80°C for the time as stated in Table 4.2. and then was polymerized further with standard polymerization conditions. Yielding styrene methacrylate block copolymers with conversions as high as 78% blocking efficiency. Root cause of variations in blocking efficiency were found to be due to amount of time the macromonomer was converted into a macro-CTA. If reaction times went too long the Macro-CTA would decompose.

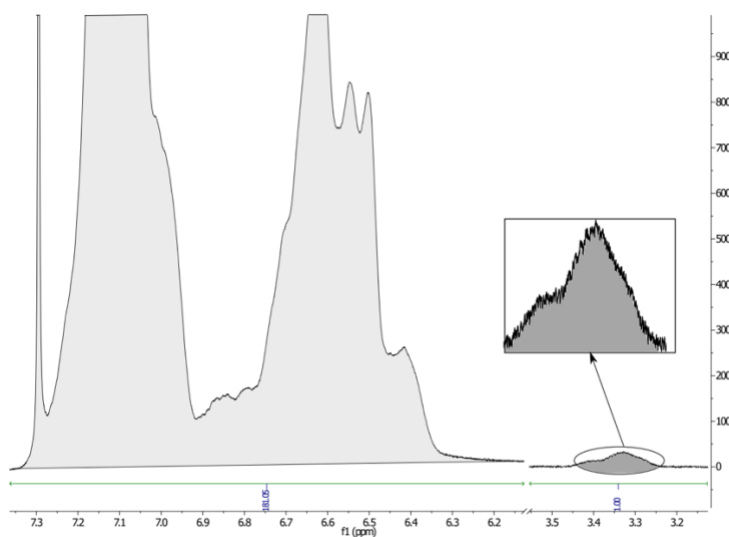


Figure 4.2. NMR showing the integration of styrene range compared to the CH₂ next to alcohol

Table 4.2. Results of macromonomer reacted with CTA over time

Reaction Time	Conversion
20	78%
40	72%
65	69%
120	54%

4.3 Conclusion

In this work we have shown that RAFT-active macro-CTAs can be efficiently produced from living polyanions under conditions that when optimized should be translatable to commercial practice. This process is done in solvents that are industrially common, as well as temperatures that are well within normal operating conditions for most industrial processes. To make this method as scalable as possible, it is desirable to reduce, replace, or remove the use of copper as the transition metal. We showed two examples working towards this end by demonstrating the ARGET method and also a photocatalytic reducing agent. While the efficiency of block-copolymer formation was low, both methods illustrated the reduction or even elimination of copper is possible with further optimization. Alternatively, macromonomer route could be used, which inherently no metals in the reaction.

While copper is usually preferred in ATRP reactions due to its nearly-ideal activation/deactivation rates, in the ATRAF method only the activation step is necessary. This means that a less-toxic/more environmentally benign transition metal with a fast activation rate such as tin, iron or titanium could potentially be substituted. If the transition metal utilization can be reduced to ppm levels while maintaining high levels of macro-CTA efficiency, we believe that ATRAF methods for producing RAFT-active materials from anionic polymerization processes could realize many of the requisite features for commercial success: high efficiency, short reaction times, and even one-pot synthesis. These features would allow for easier commercialization of RAFT polymers and would lead toward a polymer market that is more diverse in both properties and application.

4.4 Experimental

4.4.1 Polymerization of styrene

Polystyrene (PS) was produced via anionic polymerization according to commonly used procedures. Styrene and sec-butyllithium were purchased from Sigma Aldrich. Secbutyllithium (1.4M in cyclohexane) was used as received. Styrene was purified by sparging with argon and passage through an activated alumina column. HPLC grade cyclohexane (CHX) was purchased from Fisher Scientific and purified by sparging with argon and then passing over columns packed with oxygen scavenger column (Engelhard Q5) and activated alumina.

In a typical polymerization, 500 mL of CHX was added to an argon-filled round bottom flask equipped with a stir bar and septum. The flask was then heated to 40 °C in a water bath. 4.5 mL (6.3 mmol) of sec-butyllithium solution (targeting an 8 kDa polymer) was added. 50 g styrene was introduced slowly over the course of 30 min to limit the temperature increase due to the exothermic nature of the polymerization. Finally, an aliquot was taken in order to determine the molecular weight of the polymer prior to further modification.

4.4.2 PS-OH: Hydroxylation of living polystyrene

PS-OH-EO: Ethylene Oxide Capping Living polystyrene was end-capped with ethylene oxide (EO) to provide a terminal primary alcohol (PS-OH) according to established procedures.² Ethylene oxide (EO) was purchased from Sigma Aldrich and triple-purified: EO in a 10:1 molar ratio with respect to PS chains was condensed in vacuo onto calcium hydride for a 30 min to remove moisture. EO was then vacuum distilled onto 0.02 eq. of di-n-butylmagnesium and allowed to stir for an additional 30 min; this step was repeated prior to vacuum distillation to a sealed buret. The purified EO is connected to the living PS solution via a cannula, allowing vapor phase diffusion of the EO to the polymer solution. The reaction was allowed to proceed for

a 120 min and terminated with oxygen-free acidic methanol (1 mL fuming HCl:10 mL methanol).

The PS-OH solution was repeatedly washed with saturated sodium bicarbonate solution and distilled water until pH neutral. The polymer was recovered by precipitation in methanol and washed until material becomes brittle and easily broken by impact with a spatula. The material was then dried under vacuum until all traces of cyclohexane and methanol were removed. Gel permeation chromatography (GPC) analysis was used to determine the molecular weight distribution. ¹H-NMR was used to determine the extent of -OH functionalization.

NMR analysis was done by comparing the integration between 3.2-3.5 and 6.1-7.4. GPC analysis was done by integrating the peak and comparing to a polystyrene calibration.

4.4.3. Silane synthesis ((3-chloropropoxy)trimethylsilane)

All reagents were used as received. Chlorotrimethylsilane (TMSCl), 3-chloro-1-propanol and triethylamine are purchased from Sigma-Aldrich. Dichloromethane is purchased from Fisher Scientific. 1 eq of 3-chloro-1-propanol and 1.2 eq of triethylamine are mixed in DCM. 1.2 eq of TMSCl is added dropwise. Upon completion of addition the solution is allowed to stir for four hours and then purified by first removing the excess reagents and solvent. Next the mixture is distilled to yield the final product, (3-chloropropoxy)trimethylsilane. The product is confirmed by integration of NMR peak between 3.6-3.85, 1.9-2.1, .1-.3.

4.4.4. PS-OH-S: silyl capping

Living polystyrene was end-capped with (3-chloropropoxy)- trimethylsilane to provide a terminal TMS protected alcohol, which upon deprotection with tetrabutylammonium fluoride yields a primary alcohol. (3-chloropropoxy)trimethylsilane was purified by stirring over calcium hydride for several hours. A 3 eq. excess of the end terminator is added and allowed to stir for 4 hours. Upon completion of the reaction, the polystyrene is then precipitated in methanol then

dried under reduced pressure. NMR is then performed to determine end group functionality. The polymer is redissolved into cyclohexane and a 10 eq. excess of tetrabutylammonium fluoride is then added and allowed to stir for approximately 16 hours. The polymer is then precipitated and dried to give the final product. NMR analysis of silyl protected polymer was done by comparing the integration between 0.1–0.4 and 6.1–7.4. GPC analysis was done by integrating the peak and comparing to a polystyrene calibration. Analysis of the deprotected polymer (alcohol terminated) was done by observing the loss of peaks in the 0.1–0.4 region. PS-OH-A:Acetal Capping Living polystyrene was end capped with 2-(3-chloropropoxy)- tetrahydro-2H-pyran to provide a terminal acetal. The terminated is purified by stirring over calcium hydride. A 3 eq excess of the terminated is added to the living polymer solution and allowed to stir for four hours. The polymer is precipitated, dried, and NMR is used to determine end group functionality. The acetal terminated polymer is then deprotected with 1 M HCl in methanol at 65°C for 16 hours. Upon completion the polymer is precipitated, dried, and NMR is again used to determine removal of acetal functionality. 66 NMR analysis of acetal protected polymer was done by comparing the integration between 4.3–4.6 and 6.1–7.4. GPC analysis was done by integrating the peak and comparing to a polystyrene calibration. Analysis of the deprotected polymer (alcohol terminated) was done by observing the loss of peaks in the 4.3–4.6 region.

4.4.5. PS-Br: tert-bromine capping

2-bromo-2-methylpropanoyl bromide was purchased from Sigma Aldrich and used as received. 10 g of PS-OH were added to a round bottom flask with 200 mL of cyclohexane and a stir bar. After complete dissolution of the PS-OH 10 eq (with respect to chain ends) of trimethylamine was added, followed by the addition of 10 eq of 2-bromo-2-methylpropanoyl bromide over 5 min. The mixture was heated to 40 °C and allowed to react 12 h prior to precipitation and washing in methanol until brittle. The polymer was then dried under reduced

pressure to remove all traces of solvent. GPC analysis was used for molecular weight analysis and ¹H-NMR was used to confirm tertiary bromine addition by integration between 3.7-4.1.

A.1.4 PS-CTA: ATRAF Traditional ATRAF Bis(thiobenzoyl)disulfide (TBDS) and N,N,N',N'',N'''-pentamethyldiethylenetriamine (PMDETA) were purchased from Sigma Aldrich and used as received. Copper (I) bromide (CuBr) and copper wire (Cu) were acquired from Fisher Scientific and used without further purification. 1 g of the PS-Br was dissolved in 5 g toluene and degassed with 15 min of argon sparging. 2 eq TBDS, 0.1 eq CuBr, 10 eq Cu filings, and 5 eq PMDTA were added to create the catalyst complex. The solution was bubbled with argon for 15 min before the PS-Br solution was added. The mixture was then heated to 80 °C for 12 h, cooled to room temperature, and passed through a silica column to remove most of the copper. The solution was then subjected to two precipitation/dissolution cycles in 67 methanol/toluene. The polymer was then washed with methanol until brittle and then dried under vacuum overnight.

4.4.6. ARGET ATRAF method

Copper II bromide (CuBr₂) and tin (II) ethylhexanoate (SnEtH) were purchased from Sigma Aldrich and used without further purification. 1 g PS-Br was dissolved in 5 g toluene and degassed with 15 min of argon sparging. 0.3 eq CuBr₂ are dissolved in toluene and 5 eq PMDETA is added to create the copper complex. The solution was bubbled with argon for 15 min prior to the addition of the PS-Br solution. The solution is then heated to 80°C Next, 0.3 eq SnEtH was added and allowed to stir for 30 min, followed by the introduction of 0.3 eq TBDS and an additional 30 min stirring. The SnEtH/TBDS addition cycle was repeated three times. The purpose for the alternating SnEtH/TBDS addition strategy is that the SnEtH is a powerful enough reducing agent to have undesired side reactions with TBDS. Upon completion of the reaction, the polymer solution is passed through a silica column to remove most of the copper. The solution

was then subjected to two precipitation/dissolution cycles in methanol/toluene. The polymer was then washed with methanol until brittle and then dried under vacuum overnight.

4.4.7. Photocatalyzed, metal free ATRAF

10-methylphenothiazine was purchased from Sigma Aldrich and used as received. At room temperature, 1 g PS-Br was dissolved in anisole, and then 5 eq TBDS and 5 eq of methylphenothiazine were added to the solution. The mixture was bubbled for 15 min with argon prior to stirring the reaction for 20 h at room temperature while being subjected to 254 nm wavelength light in a Southern New England Ultraviolet Company Photochemical Reactor with a RPR 3000A bulb.

4.4.8. PS-Acrylate block copolymers: PS-CTA mediated RAFT polymerization of acrylates

All acrylate monomers were purchased from sigma-aldrich and were used as received.

N-Butyl acrylate 0.1 g of PS-CTA (8 kDa, 12.5 μmol), 1 g toluene, 0.4 g of n-butyl acrylate (3.13 mmol), and 0.492 mg of AIBN (3 μmol) were added to a flask and purged with argon for 10 min, and then heated to 80 °C for 1 h. The mixture was cooled, and the resultant poly(styrene-block-n-butyl acrylate) (PS-nBA) block copolymer was recovered by evaporation of toluene and unreacted butyl acrylate under vacuum. The polymer is then analyzed using GPC in order to determine the percent cross-over from PS to PS-CTA. This is done by integrating the UV signal of the grown polymer peak and integrating the residual original polymer peak. The ratio of the two yields the conversion.

The efficiency of the ATR reaction is determined by producing a block co-polymer of the styrene with NBA and using a UV detector to determine the amount of styrene that is present in the block-copolymer and comparing this to the residual original styrene peak.

Methyl methacrylate 0.1 g of PS-CTA (8 kDa, 12.5 μmol), 1 g toluene, 0.4 g of methyl methacrylate (4 mmol), and 0.492 mg of AIBN (3 μmol) were added to a flask and purged with argon for 10 min, and then heated to 80 °C for 1 h. The mixture was cooled, and the resultant poly(styrene-block-methyl methacrylate) (PS-MMA) block copolymer was recovered by evaporation of toluene and unreacted methyl methacrylate under vacuum. The polymer is then analyzed using GPC in order to determine the percent cross-over from PS to PS-CTA. This is done by integrating the UV signal of the grown polymer peak and integrating the residual original polymer peak. The ratio of the two yields the conversion.

The efficiency of the ATR reaction is determined by producing a block co-polymer of the styrene with methyl methacrylate and using a UV detector to determine the amount of styrene that is present in the block-copolymer and comparing this to the residual original styrene peak. This will allow for the calculation of end-capping efficiency.

Methyl acrylate 0.1 g of PS-CTA (8 kDa, 12.5 μmol), 1 g toluene, 0.4 g of methyl acrylate (4.64 mmol), and 0.492 mg of AIBN (3 μmol) were added to a flask and purged with argon for 10 min, and then heated to 80 °C for 1 h. The mixture was cooled, and the resultant poly(styrene-block-methyl acrylate) (PS-MA) block copolymer was recovered by evaporation of toluene and unreacted methyl acrylate under vacuum. The polymer is then analyzed using GPC in order to determine the percent cross-over from PS to PS-CTA. This is done by integrating the UV signal of the grown polymer peak and integrating the residual original polymer peak. The ratio of the two yields the conversion.

The efficiency of the ATR reaction is determined by producing a block co-polymer of the styrene with NBA and using a UV detector to determine the amount of styrene that is present in the block-copolymer and comparing this to the residual original styrene peak.

4.4.10. Gel permeation chromatography (GPC)

GPC was done on a Waters Acquity APC System, equipped with a RI and UV detector. The columns used were XT 125, 200, 450, and 900. The system runs at 1 mL/min in tetrahydrofuran.

4.4.11. Nuclear magnetic resonance spectroscopy (¹H-NMR)

Volume fraction of PS-PMA and the end group functionalization was calculated based on ¹H NMR spectra recorded in deuterated chloroform with a Bruker Avance III spectrometer (600 MHz).

4.4.12. Differential scanning calorimetry (DSC)

The DSC measurement was taken from TA DSC Q2000 differential scanning calorimeter operating under nitrogen atmosphere. Samples underwent two cycles of heating and cooling process at 20°C/min and 10°C/min, respectively. The glass transition temperatures (T_g s) were taken from the second heating cycle.

4.4.13. Transmission electron microscopy (TEM)

Before proceeding viscoelastic behavior and transmission electron microscope (TEM) micrographs, samples were annealed at 100°C under vacuum for 3 days. To obtain ultrathin sections of sample for TEM imaging, PS-PMA was cut into 70 nm thick sections by cryomicrotome at -50°C. The contrast of two blocks under TEM was enhanced by selective staining of osmium tetroxide which stained methyl acrylate only. TEM micrographs were then taken by FEI Tecnai G2-F20 scanning transmission electron microscope operating at 200 kV. The black and white regions were PMA and PS, respectively.

4.4.14. Dynamic shear rheology (DSR)

The viscoelastic behavior of PS-PMA was tested by a TA ARES-G2 rheometer. Sample was thermally pressed into 1 mm thick disk before testing. Both isochronal test and temperature

frequency sweep were performed on 8 mm parallel plates. Data points shown in isochronal test were taken every 5 °C during heating under a constant 4% shear strain and 1 rad/s angular frequency oscillation. To acquire the master curve, temperature frequency sweep was performed between 40 and 160 °C and oscillated between 1 and 100 rad/s in the viscoelastic region of sample. Data points were then shifted corresponding to the principle of time-temperature superposition.

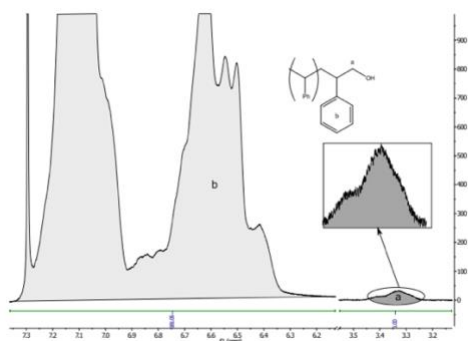


Figure 4.3. NMR showing the integration of styrene range compared to the CH₂ next to alcohol. The ratio of these peaks gives a rough estimate of the number of alcohol functional groups present.

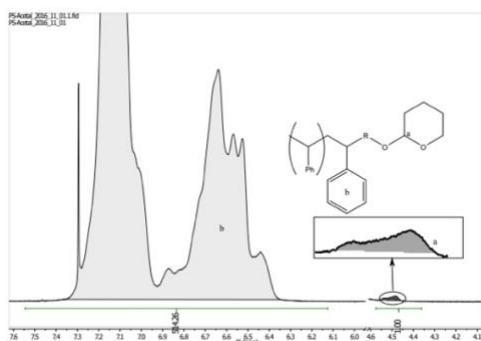


Figure 4.4. ¹H-NMR showing the region associated with the acetal proton. The ratio of this peak to the styrene peak gives a rough estimate of the number of acetal functional groups present.

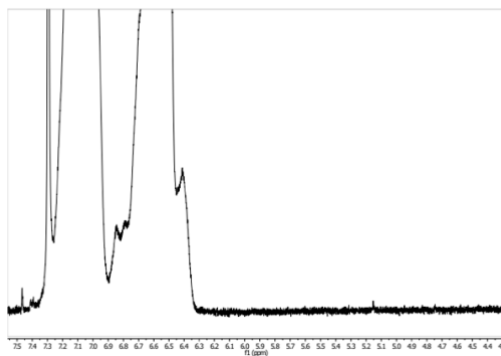


Figure 4.5. $^1\text{H-NMR}$ showing the lack of peaks in the acetal proton region. This is a strong indication that we have removed the acetal functionality and replaced it with a primary alcohol.

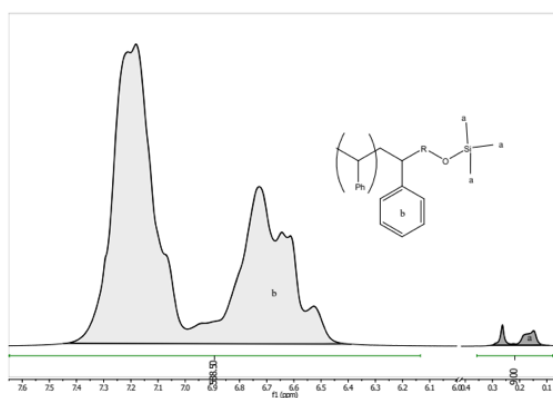


Figure 4.6. $^1\text{H-NMR}$ showing the region associated with the silyl methyl proton. The ratio of this peak and the styrene peak gives a rough estimate of the number of silyl functional groups present

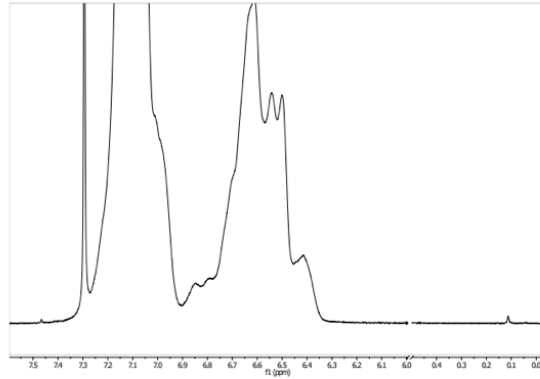


Figure 4.7. ^1H -NMR showing the lack of peaks in the silyl methyl proton region. This demonstrates that we were able to cleave the silyl functional group and leave behind a primary alcohol.

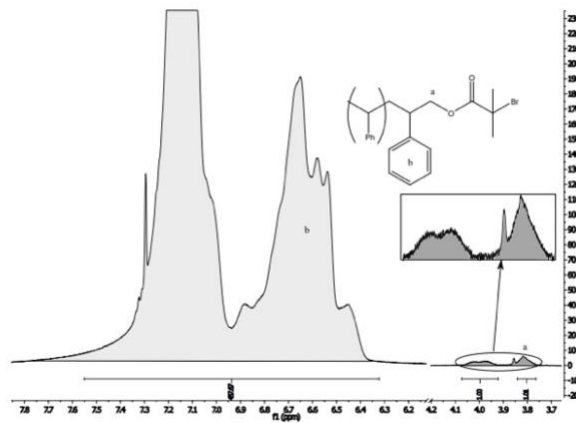


Figure 4.8. NMR showing the integration of styrene range compared to the CH_2 next to the tert-butyl bromide ester. The ratio of these integrals gives a rough estimate of how many tertiary bromide functional groups are present.

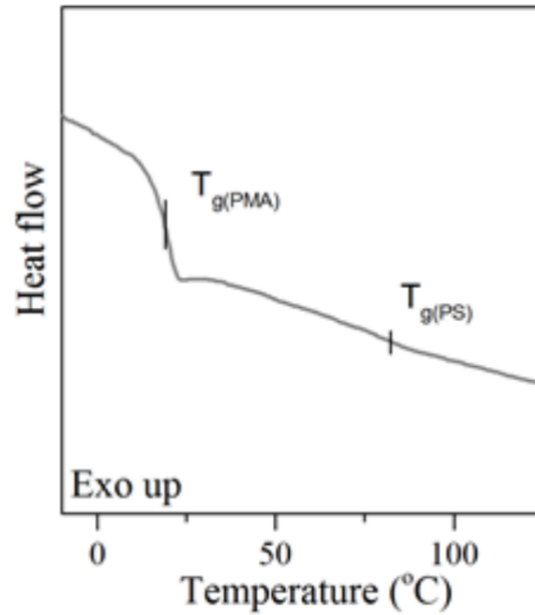


Figure 4.9. DSC showing glass transition of both methyl acrylate as well as polystyrene blocks. While the polystyrene glass transition is weak, both the PS and the PMA glass transitions have shifted inward from where they would be for homopolymers. This is strong indication of the production of a block copolymer.

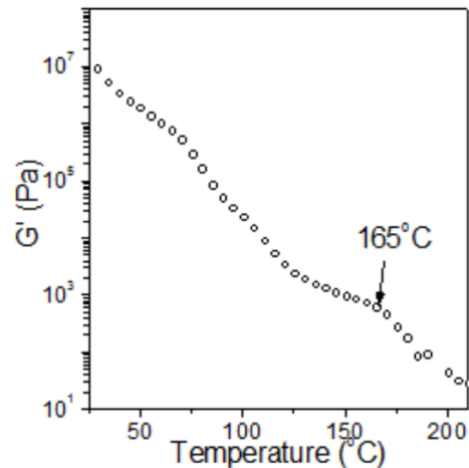


Figure 4.10. Isochronal rheology temperature ramp that shows an order to disorder transition at 165°. This is further evidence that the styrene was converted to a styrenic acrylate copolymer.

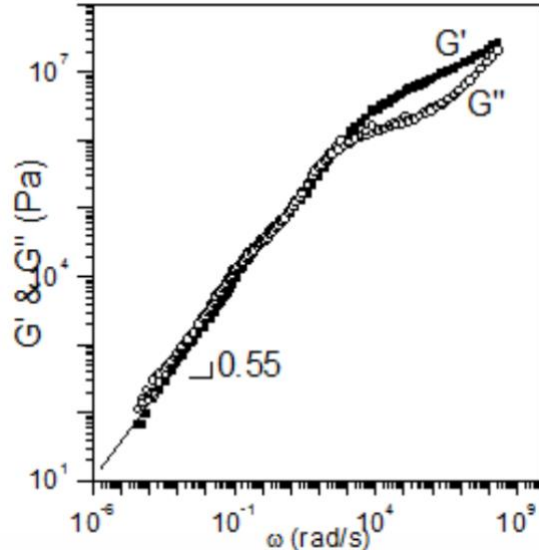


Figure 4.11. Rheology master curve done on block co-polymer showing a terminal slope of 0.55. This is typically of lamellar phase separated block copolymers and is a strong indication that the styrene was converted to a block copolymer

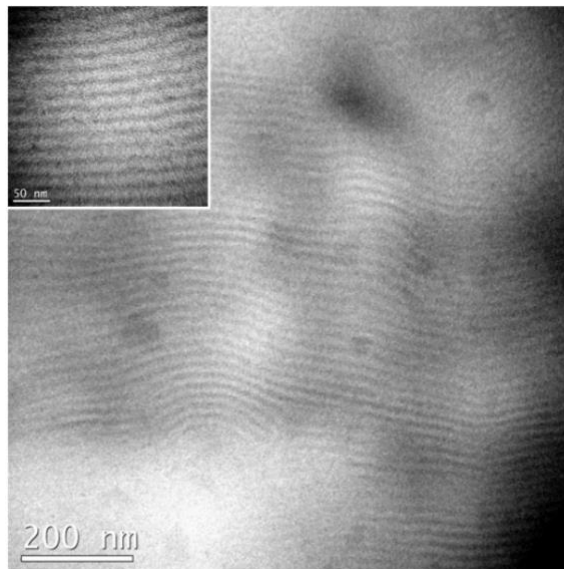


Figure 4.12. TEM showing the phase separation between the methyl acrylate and styrene blocks. This shows very clear lamellar phase separation and is confirmation of the production of a block copolymer

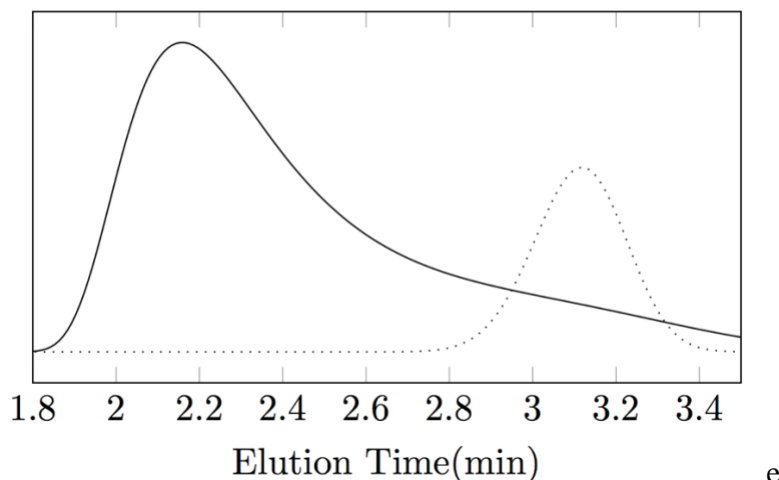


Figure 4.13. GPC showing the growth of PS-NBA(solid line) and unmodified PS (dashed line)

4.5 References

- [1] Szwarc, M. Living polymers and mechanisms of anionic polymerization. In *Living Polymers and Mechanisms of Anionic Polymerization*, pages 1–177. Springer 1983.
- [2] Li, X.; Marasteanu, M. The fracture process zone in asphalt mixture at low temperature. *Engineering Fracture Mechanics* **2010**, 77(7):1175–1190.
- [3] Chi-Chen Hsieh, H.; Huang, C. H.; Lin, F.; Lee, P. J. D. Rubber for a high-performance tire tread, October 17 **2000**. US Patent 6, 133, 376.
- [4] Fayt, R.; Forte, R.; Jacobs, C.; Jérôme, R.; Ouhadi, T.; Teyssié, P.; Varshney, S. K.; New initiator system for the living anionic polymerization of tert-alkyl acrylates. *Macromolecules* **1987**, 20(6): 1442–1444.
- [5] Matyjaszewski, K. Atom transfer radical polymerization (atrp): current status and future perspectives. *Macromolecules* **2012**, 45(10): 4015–4039.
- [6] Mueller, L.; Jakubowski, W.; Matyjaszewski, K.; Pietrasik, J.; Kwiatkowski, P.; Chaladaj, W.; Jurczak J. Synthesis of high molecular weight polystyrene using agat atrp under high pressure. *European Polymer Journal* **2011**, 47(4): 730–734.
- [7] Zhang, L.; Cheng, Z.; Shi, S.; Li, Q.; Zhu, X. Agat atrp of methyl methacrylate catalyzed by fecl₃/iminodiacetic acid in the presence of air. *Polymer* **2008**, 49(13-14): 3054–3059.

- [8] Min, K.; Gao, H.; Matyjaszewski, K. Use of ascorbic acid as reducing agent for synthesis of well-defined polymers byARGET ATRP. *Macromolecules* **2007**, 40(6): 1789–1791.
- [9] Konkolewicz, D.; Magenau, A. J. D.; Averick, S. E.; Simakova, A.; He, H.; Matyjaszewski, K. Icar ATRP with ppm Cu catalyst in water. *Macromolecules* **2012**, 45(11): 4461–4468.
- [10] Nicolaÿ, R.; Kwak, Y.; Matyjaszewski, K. A green route to well-defined high-molecular-weight (co)polymers usingARGET ATRP with alkyl pseudohalides and copper catalysis. *Angewandte Chemie* **2010**, 122(3): 551–554.
- [11] Moad, G.; Rizzardo, E.; Thang, S. H. Living radical polymerization by the RAFT process—a third update. *Australian Journal of Chemistry* **2012**, 65(8): 985–1076.
- [12] Renzhong Wei, Yingwu Luo, and Zhengshang Li. Synthesis of structured nanoparticles of styrene/butadiene block copolymers via RAFT seeded emulsion polymerization. *Polymer* **2010**, 51(17): 3879–3886.
- [13] Durrieu, F.; Farcas, F.; Mouillet, V. The influence of UV aging of a styrene/butadiene/styrene modified bitumen: comparison between laboratory and on site aging. *Fuel* **2007**, 86(10): 1446–1451.
- [14] Galán, C.; Sierra, C. A.; Fatou, J. M.; Delgado, J. A. A hot-melt pressure-sensitive adhesive based on styrene–butadiene–styrene rubber. The effect of adhesive composition on the properties. *Journal of Applied Polymer Science* **1996**, 62(8): 1263–1275.
- [15] Jubete, E.; Liauw, C. M.; Allen, N. S. Water uptake and tensile properties of carboxylated styrene butadiene rubber based water born paints: models for water uptake prediction. *Progress in Organic Coatings* **2007**, 59(2): 126–133.
- [16] Zhang, C.; Yang, Y.; He, J. Direct transformation of living anionic polymerization into RAFT-based polymerization. *Macromolecules* **2013**, 46(10): 3985–3994.
- [17] Xu, J.; He, J.; Fan, D.; Tang, W.; Yang, Y. Thermal decomposition of dithioesters and its effect on RAFT polymerization. *Macromolecules* **2006**, 39(11): 3753–3759.
- [18] Yin, L.; Dalsin, M. C.; Sizovs, A.; Reineke, T. M.; Hillmyer, M. A. Glucose-functionalized, serum-stable polymeric micelles from the combination of anionic and RAFT polymerizations. *Macromolecules* **2006**, 45(10): 4322–4332.
- [19] Kwak, Y.; Nicolaÿ, R.; Matyjaszewski, K. Synergistic interaction between ATRP and RAFT: Taking the best of each world < a class. *Australian Journal of Chemistry* **2009**, 62(11): 1384–1401.

- [20] Treat, N. J.; Sprafke, H.; Kramer, J. W.; Clark, P. G.; Barton, B. E.; de Alaniz, J. R.; Fors, B. P.; Hawker, C. J. Metal-Free Atom Transfer Radical Polymerization. *Journal of the American Chemical Society* **2014**, 136(45): 16096–16101.
- [21] Houshyar, S.; Keddie, D. J.; Moad, G.; Mulder, R. J.; Saubern, S.; Tsanaktsidis, J. The scope for synthesis of macro-raft agents by sequential insertion of single monomer units. *Polymer Chemistry* **2012**, 3(7): 1879–1889.

CHAPTER 5. GENERAL CONCLUSION

This work focused on using bio-based molecules for industrial applications and the development of chemical methodology of γ -pyrones. Chapter 1 emphasizes the conversion of TAL into new applications. The corrosion inhibitors were synthesized from TAL in two steps. This process showed efficient corrosion inhibitors can be developed from TAL in good yields. Some corrosion inhibitors produced had a higher corrosion inhibitor efficiency than both the heterocycle base and the standard. Further work will be needed to determine the mechanism to better understand corrosion inhibitor efficiency.

In chapter 2 a new methodology for γ -pyrones was described. Acid chlorides reacted with 1,3-dicarbonyl compounds to produce γ -pyrones. This method allowed for a new route to 5-hydroxychomanones, which can be designed for new medicinal applications.

In chapter 3 the applications of citric and malic acid and reactions were explored. Mixtures of citric acid and malic acid reacted to produce a pyrone diacid. The pyrone can be regioselectively converted to the monoacid. Methyl malate and methyl citrate mixtures can also react to form a diester pyrone. These mixtures of citric and malic acid could be further transformed into plasticizers that are competitive with petroleum phthalate-based plasticizers.

In chapter 4 the marriage of anionic and RAFT polymerization methods in a scalable fashion led to the synthesis of block copolymers. The new method was designed to synthesize block copolymers with the cost of large-scale product development in mind. Polystyrene was blocked with a rubbery acrylate block to add stiffness to the overall polymer. While it does not eliminate petroleum-based mass from styrene, it does significantly increase the amount of bio-based mass used in petroleum-based applications. An attempt was made to lower the cost of the synthesis, allowing for new applications of this system.